HAL
open science

The interaction of N2O5 with mineral dust: aerosol flow tube and Knudsen reactor studies

C. Wagner, F. Hanisch, N. Holmes, H. de Coninck, G. Schuster, J. N. Crowley

To cite this version:

C. Wagner, F. Hanisch, N. Holmes, H. de Coninck, G. Schuster, et al.. The interaction of N2O5 with mineral dust: aerosol flow tube and Knudsen reactor studies. Atmospheric Chemistry and Physics, 2008, 8 (1), pp.91-109. hal-00296409

HAL Id: hal-00296409

https://hal.science/hal-00296409v1

Submitted on 18 Jun 2008

HAL is a multi-disciplinary open access archive for the deposit and dissemination of scientific research documents, whether they are published or not. The documents may come from teaching and research institutions in France or abroad, or from public or private research centers.

L'archive ouverte pluridisciplinaire **HAL**, est destinée au dépôt et à la diffusion de documents scientifiques de niveau recherche, publiés ou non, émanant des établissements d'enseignement et de recherche français ou étrangers, des laboratoires publics ou privés.

Atmos. Chem. Phys., 8, 91–109, 2008
www.atmos-chem-phys.net/8/91/2008/
© Author(s) 2008. This work is licensed
under a Creative Commons License.

Atmospheric Chemistry and Physics

The interaction of N_2O_5 with mineral dust: aerosol flow tube and Knudsen reactor studies

C. Wagner[1], F. Hanisch[1,*], N. Holmes[1,], H. de Coninck[1,***], G. Schuster[1], and J. N. Crowley[1]**

[1]Max-Planck-Institut für Chemie, Mainz, Germany
[*]now at: Bayerisches Staatsministerium für Umwelt, Gesundheit und Verbraucherschutz, Rosenkavalierplatz 2, 81925 München, Germany
[**]now at: International Laboratory for Air Quality and Health, QUT Gardens Point, 2 George Street, Brisbane, 4001 QLD, Australia
[***]now at: Unit Policy Studies of the Energy research Centre of the Netherlands, (ECN), VU University of Amsterdam (IVM), Radarweg 60, 1040 AW Amsterdam, The Netherlands

Received: 7 September 2007 – Published in Atmos. Chem. Phys. Discuss.: 12 September 2007
Revised: 5 December 2007 – Accepted: – Published: 14 January 2008

Abstract. The interaction of mineral dust with N_2O_5 was investigated using both airborne mineral aerosol (using an aerosol flow reactor with variable relative humidity) and bulk samples (using a Knudsen reactor at zero humidity). Both authentic (Saharan, SDCV) and synthetic dust samples (Arizona test dust, ATD and calcite, $CaCO_3$) were used to derive reactive uptake coefficients (γ). The aerosol experiments (Saharan dust only) indicated efficient uptake, with e.g. a value of γ(SDCV)=(1.3±0.2)×10^{-2} obtained at zero relative humidity. The values of γ obtained for bulk substrates in the Knudsen reactor studies are upper limits due to assumptions of available surface area, but were in reasonable agreement with the AFT measurements, with: γ(SDCV)=(3.7±1.2)×10^{-2}, γ(ATD)=(2.2±0.8)×10^{-2} and γ($CaCO_3$)=(5±2)×10^{-2}. The errors quoted are statistical only. The results are compared to literature values and assessed in terms of their impact on atmospheric N_2O_5.

1 Introduction

Estimates of emissions of mineral dust into the atmosphere presently lie at somewhat less than 2000 Tg per annum (Lunt and Valdes, 2002; Tegen et al., 2002; Luo et al., 2003) making it an important component of the coarse fraction of atmospheric aerosol and explaining its significant impact on several aspects of atmospheric science including radiative forcing, and modification of photochemical cycles. The direct radiative forcing effect (due to scattering and absorption of incoming solar radiation) is accompanied by an indirect effect as clay and silica particles are effective condensation and ice nuclei (Sassen et al., 2003; Ansmann et al., 2005), which can ultimately affect cloud structure and precipitation patterns (Twomey et al., 1984). The latter effect will likely be modified by the physical state of the mineral dust particles, which will be influenced by chemical ageing during atmospheric transport. Evidence from field, laboratory and modelling efforts is increasing pointing towards an important role of mineral dust as provider of reactive surfaces for several trace gases. Interaction of mineral dust with atmospheric NO_x-NO_y trace gases is particularly interesting due to its potential impact on photochemical ozone production. An increase in the nitrate content of dust during transport over polluted regions has been documented on several occasions (Nishikawa and Kanamori, 1991; Silva et al., 2000; Mori et al., 2003; Hwang and Ro, 2005; Matsuki et al., 2005) and model studies have confirmed that this is consistent with the uptake of reactive NO_y traces gases such as HNO_3 and N_2O_5 (Carmichael et al., 1996; Dentener et al., 1996).

The overall impact which heterogeneous reactions of NO_y on mineral aerosol exert on tropospheric photochemical cycles, has been assessed in several combined aerosol/gas-phase models (Zhang et al., 1994; Dentener et al., 1996; Phadnis and Carmichael, 2000; Song and Carmichael, 2001; Bian and Zender, 2003; Bauer et al., 2004). All models suggest a significant impact of NO_y uptake on e.g. the partitioning of nitrate between the gas and particulate phase, the NO_y/NO_x ratio and ozone concentrations.

Correspondence to: J. N. Crowley
(crowley@mpch-mainz.mpg.de)

Published by Copernicus Publications on behalf of the European Geosciences Union.

N_2O_5 is generated in the termolecular reaction of NO_2 with NO_3, which is formed mainly by the reaction of NO_2 with O_3 (R1)

$$NO_2 + O_3 \rightarrow NO_3 + O_2 \quad \text{(R1)}$$

$$NO_2 + NO_3 + M \rightarrow N_2O_5 + M \quad \text{(R2)}$$

Although the fast photolysis of NO_3 (lifetime is $\approx$1 s) (Wayne et al., 1991) renders N_2O_5 formation inefficient during the day, N_2O_5 can be an important reservoir of NO_3 and NO_2 during night-time. At night, the relative concentrations of N_2O_5, NO_3 and NO_2 are controlled by the equilibrium described by the formation of N_2O_5 (R1, R2) and its loss due to thermal decomposition (R-2):

$$N_2O_5 + M \rightarrow NO_2 + NO_3 + M \quad \text{(R-2)}$$

This equilibrium can be perturbed by changes in concentration of any one of the three trace gases, with loss of N_2O_5 expected to be important due to the well established reactivity of this acid anhydride towards aqueous or moist surfaces, resulting in nitrate formation (R3). The long photochemical lifetime and high solubility of nitrate/nitric acid result in large deposition rates and permanent removal from the atmosphere.

$$N_2O_5 + \text{surface} + H_2O \rightarrow 2HNO_3 \ \text{(or nitrate)} \quad \text{(R3)}$$

The loss of N_2O_5 on an aerosol is thus recognised as an important removal process for NO_x in many regions of the atmosphere (Chartrand and McConnell, 1999; Hendricks et al., 1999; Evans and Jacob, 2005). The direct reduction in NO_3 and the indirect reduction of O_3 (due to repartitioning of NO_x to NO_y) both impact on the oxidising power of the troposphere.

The rate of (R3) is determined by the available aerosol surface area and the efficiency of the trace-gas aerosol interaction, the latter being described by the uptake coefficient, γ. Using values of γ of $\approx$0.1, early modelling studies established an important role for reaction (R3) on aqueous surfaces (Dentener and Crutzen, 1993) though the effect is still significant with the presently preferred values of γ which are closer to 0.02 (Evans and Jacob, 2005).

In the absence of experimental data on the efficiency of uptake of N_2O_5 to a mineral dust surface, previous efforts to model the effect of this process have used values of γ which reveal a large spread: Dentener et al. (1996) used γ=0.1 based on the data available for aqueous surfaces at that time whilst Zhang et al. (1994) allowed γ to vary between 0.01 and 1. More recently, values of γ=0.03, 0.01 and 0.001 have been used by Shon et al. (2004), Evans and Jacob (2005) and Bian and Zender (2003), respectively. Bauer et al. (2004) employed a value of γ that varied between 0.02 and 0.003 depending on relative humidity.

Experimental data which has been published since these modelling studies does not help to resolve the issue, as two separate studies using essentially the same experimental method, and both using Saharan dust samples have derived values of the uptake coefficient as diverse as 0.01 (Seisel et al., 2005) and 0.2. (Karagulian et al., 2006) Both Seisel et al. (2005) and Karagulian et al. (2006) carried out experiments using porous, bulk substrates and Knudsen reactors, which can lead to large uncertainty in estimation of the surface area available for reaction and which do not allow variation of relative humidity. In order to overcome the limitations posed by the Knudsen reactor approach we have conducted experiments using an aerosol flow reactor with dispersed, authentic Saharan dust from the Cape Verde islands (SDCV). In addition to removing the problems associated with the use of bulk samples, this approach also enabled experiments to be conducted under different relative humidities. We compare our results using the aerosol flow reactor to our Knudsen reactor experiments using SDCV, Arizona test dust (ATD), and calcite ($CaCO_3$), and to the two previous literature values.

2 Experimental section

Two distinctly different set ups have been used to investigate the interaction of N_2O_5 with mineral dust. Similar to our previous work on HNO_3 (Hanisch and Crowley, 2001b), we used a Knudsen reactor to investigate the uptake to bulk samples under conditions of low humidity, whilst uptake to airborne mineral aerosol was investigated using an aerosol flow tube, both operated at the laboratory temperature of 296±2 K. The aerosol flow tube is described here for the first time so a detailed technical description is given. The Knudsen reactor has been described previously (Hanisch and Crowley, 2001b) and only salient features and operational parameters are mentioned here.

2.1 Aerosol flow tube

2.1.1 Gas flow characteristics

The aerosol flow tube (AFT, Fig. 1) is a vertically mounted Pyrex tube of length 120 cm and internal diameter 4 cm. Aerosol can be introduced into the top of the AFT via a side arm, whereas trace gases are introduced axially into the centre of the AFT via a stainless steel, movable injector (6 mm OD), the position of which defines the contact time between trace gases and aerosol or reactor walls. N_2O_5 is flown through the stainless steel injector through a 1/8th inch Teflon pipe and only has contact with the last 10 cm of the injector, which is coated with a thin Teflon film (Dupont, FEP). The AFT is usually operated at or close to atmospheric pressure to reduce loss of N_2O_5 to the walls, which, combined with total gas flows of 3 L (STD) min^{-1} (SLM) N_2 result in a Reynolds number of 110 and an entrance length to acquire laminar flow of $\approx$25 cm.

Most experiments were carried out using an aerodynamic particle sizer (see below) which operates at a flow of 5 SLM,

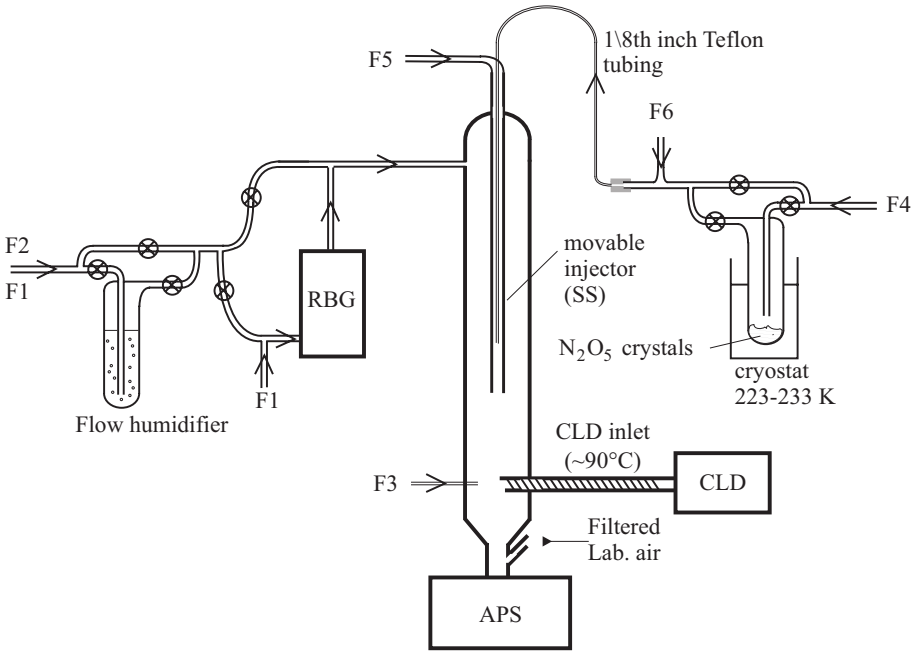

Fig. 1. Aerosol flow tube set-up. RBG = rotating brush generator, CLD = chemiluminescence NO detector, APS = aerodynamic particle sizer spectrometer, SS = stainless steel. The total flow (N_2 unless otherwise stated) was 3000 sccm with (typically) F4+F6=500 sccm; F5=10 sccm; F3=20 sccm (0.001% NO in N_2); F1+F_2=2500 sccm (with a variable proportion through the humidifier to obtain RH of 0, 29 and 58%).

so that an addition 2 SLM of filtered (particle free) laboratory air, was mixed into the 3 SLM reactor flow downstream of the reactor (see Fig. 1). The total reactor flow comprised of 2.5 SLM carrying the aerosol (partly passing through the aerosol generator (see below) and partly passing through a bubbler containing water for humidification of the flow) and 0.5 SLM via the injector. By variation of the flow through the bubbler, the experimental relative humidity (RH) was set at 0, 29 or 58%. Other minor flows e.g. 10 cm^3 (STD) min^{-1} (sccm) injector purge are indicated in Fig. 1.

Mixing of trace gas flowing from the injector with the bulk flow was observed by adding NO_2 to the injector and measuring its concentration at various fixed distances from the inlet to the detector (see below). Well mixed flows were observed at distances greater than ≈25 cm from the injector. At 3 SLM total flow rate the average linear velocity was ≈4 cm s^{-1}, resulting in a maximum trace gas residence time of ≈30 s. The validity of calculating the average velocity via total flow rates and pressure could be confirmed by adding a pulse of gas (NO_2) to the injector and monitoring its average time of arrival at the detector.

2.1.2 Generation and detection of N_2O_5

N_2O_5 was eluted via the injector into the flow tube by passing a stream of N_2 (usually 20–80 sccm, F4) over N_2O_5 crystals held at 223 K and dynamically diluting this flow with further 480–420 sccm N_2 (F6). The complete injector flow (500 sccm) was transported through 1/8th inch Teflon piping (≈1.5 m) into the lower 10 cm of the injector (i.d. 5 mm) and then into the flow tube. The vapour pressure of N_2O_5 at 223 K is ≈0.25 Torr (Fahey et al., 1985) which, assuming saturation of the N_2 flow, results in N_2O_5 concentrations in the injector of $\approx 10^{13}$–10^{14} molecule cm^3. Mixing of the injector flow (500 sccm) with the main gas flow (2.5 SLM) results in flow tube concentrations of N_2O_5 between 5×10^{12} and 5×10^{13} molecule cm^{-3}, which were necessary for reasons related to the N_2O_5 detection scheme (see below). As shown by Reactions (R2) and (R-2), N_2O_5 is in dynamic equilibrium with NO_2 and NO_3, thus the N_2O_5 source will also contain these "impurities". Using evaluated (Sander et al., 2006) equilibrium constants and rate coefficients for (R2) and (R-2) it is easy to show that at 223 K (the temperature of the N_2O_5 crystals) the equilibrium favours N_2O_5 formation so that its concentration is a factor $\approx 10^6$ greater than NO_3 and NO_2. However, during transport through the injector the gas is warmed to room temperature and N_2O_5 (initially at $\approx 10^{14}$ molecule cm^{-3}) decomposes to generate NO_3 and NO_2 at ≈1% level in ≈1 s. Dilution in the main flow results e.g. in a concentration of N_2O_5 close to 1×10^{13} molecule cm^{-3} and equilibrium concentrations of NO_3 and NO_2 of 5×10^{11} molecule cm^3, equilibrium being achieved in ≈2 s. The presence of NO_2 and NO_3 impurities in the flow tube at these low levels has no significant impact on N_2O_5 detection, though we later discuss the potential role which the dynamic equilibrium between N_2O_5, NO_3 and NO_2 may have on the determination of N_2O_5 loss rates.

N_2O_5 was detected using a modified chemiluminescence detector (CLD). Conventionally, CLD devices are used to detect NO_y and NO_x via thermal conversion (in an oven at several hundred °C) to NO, which is detected via the generation of chemiluminescence (NO_2* emission) from its reaction with O_3. To detect N_2O_5 selectively in the presence of potential impurities such as NO_2 and HNO_3 we make use of the fact that N_2O_5 is thermally unstable and dissociates to NO_3 and NO_2 rapidly at temperatures well below 100°C whereas HNO_3 and NO_2 do not. At 90°C and atmospheric pressure, the lifetime of N_2O_5 with respect to thermal dissociation is $\approx 5\times10^{-2}$ s and the NO_3 product of the thermal dissociation reacts rapidly with NO (k_4 (363 K)=2.4×10^{-11} cm^3 molecule^{-1} s^1(Sander et al., 2006)):

$$NO_3 + NO \rightarrow 2NO_2 \quad \text{(R4)}$$

The inlet to the CLD (see Fig. 1) consisted of a heated length (≈10 cm) of 5 mm i.d. Teflon tubing (at 90°C) to thermally dissociate N_2O_5 and a flow of NO which could be monitored directly by the CLD (i.e. without the oven). NO was introduced using 1/8th inch stainless steel piping close to the inlet as shown in Fig. 1.

N_2O_5 was thus monitored as the change in NO concentration at the detector. 120 sccm of gas were sampled into the heated Teflon tube, resulting in residence times of about 1 s. This residence time, during which all N_2O_5 should decompose (R-2) and all NO_3 should react with NO, placed some constraint on the lower bound to the concentrations of NO and N_2O_5 which could be used. Also, it was desirable to convert N_2O_5 as rapidly as possible to minimise reactions on surfaces that, during an experiment, could change their reactivity towards N_2O_5 due to the deposition of mineral aerosol. Numerical simulation of Reactions (R2), (R-2) and (R4) at 90°C showed that concentrations close to 10^{13} molecule cm^{-3} of N_2O_5 and [NO]/[N_2O_5]=1.1 resulted in a NO response that equalled the initial N_2O_5 concentration and which took place in just 2–3 cm (i.e. within 0.3 s) of the heated Teflon inlet. By calibration of the CLD using a known NO concentration we thus measured the N_2O_5 concentration with ≈10% accuracy.

The large conversion rate of NO_3 to NO_2 via (R4) also minimises potential loss of NO_3 via its thermal dissociation to NO and O_2 (R5), which has been reported to proceed with a time constant of ≈7 s at 90°C (Wayne et al., 1991).

$$NO_3 + M \rightarrow NO + O_2 + M \quad \text{(R5)}$$

Experimental tests of the detector set-up, including linearity of response to NO, the lack of NO modulation by added N_2O_5 when the heater was cold (confirming the low, (i.e. 5%) equilibrium concentrations of NO_3 at room temperature as described above) and lack of detector response to N_2O_5 in the absence of added NO confirmed the suitability of this approach. In addition, variation of the inlet temperature whilst monitoring a constant concentration of N_2O_5 confirmed that 90°C was the optimal operational temperature.

2.1.3 Generation and characterisation of mineral aerosol

Mineral dust was available in the form of bulk samples of Saharan dust (SDCV), the mineralogy/composition of which have been described in our previous publications (Hanisch and Crowley, 2001a; Hanisch and Crowley, 2001b; Hanisch and Crowley, 2003b; Hanisch and Crowley, 2003a) and is not repeated here. SDCV samples were dispersed and entrained in N_2 using a commercial rotating brush generator (Palas, RBG). Using the RBG we were able to produce gas flows containing up to several thousand particles per cm^3 in the flow tube, providing sufficient surface area for N_2O_5 uptake and reaction on the ≈10–30 s time scale of the experiments. An aerosol impactor located close to the output of the RBG removed particles of diameters greater than a few μm.

The number and size distribution of particles in the reactor was monitored using a aerodynamic particle sizer spectrometer, APS (TSI-3321), located downstream of the flow tube and which sampled the complete 3 SLM flow (and an additional 2 SLM of lab air, containing no particles in that size range, see above). The APS measures particles in the size range 0.5 to 17 μm and was thus suitable for the coarse mineral aerosol particles studied in this work. The use of high particle concentrations required employment of a dilution stage (factor 20) in the APS (TSI-3302A). The APS works on the time of flight principle to derive an equivalent aerodynamic particle diameter (D_a), defined as the diameter of a spherical particle of unit density (ρ) with identical aerodynamic properties. The aerodynamic diameter can be corrected for non-unity density to derive the Stokes equivalent diameter (Hinds, 1999) (D_s) which can be used to calculate e.g. the surface area of a spherical particle.

$$D_s = D_a\sqrt{\frac{1}{\rho}} \quad (1)$$

The calibration of the APS was tested using spherical Latex particles (provided by TSI) with nominal diameters of 7.24 and 10.98 μm which have a density of 1 g cm^{-3}, so that D_s=D_a. The APS measured these particles reliably, returning diameters of 7.7 and 11.1 μm, respectively, a deviation of less than 6%. The accuracy of the APS in the small particle range was tested with spherical SiO_2 particles of known diameter (determined by scanning electron microscope). Once corrected for the density of the SiO_2 spheres, the APS measured diameters of 430, 890 and 1200 nm for the nominally 500, 1000 and 1400 nm particles, respectively indicating deviations of 10–15%.

A SDCV particle distribution obtained using the APS is given in Fig. 2. The distribution maximises at an aerodynamic diameter of 1.5 μm, which is in good agreement with an independent analysis using a loaned, electrical low

pressure impactor (Dekati Ltd.), which measured an aerodynamic diameter of between 1 and 2 μm. In addition, Inspection by scanning electron microscopy of SDCV particles collected on an impactor from the reactor indicate that non-agglomerated particles indeed have a diameter which is close to 1 μm.

Once corrected for the SDCV density of 2.7 g cm^{-3} (Hanisch and Crowley, 2003b), the APS data result in a Stokes average diameter of 0.85 μm. The APS provides both analogue output related to the number of particles per cm^3, and also a time averaged size distribution. Typically the size distribution was recorded every 2 s whilst the number of particles was recorded continuously and over the same time period as the N_2O_5 signal was acquired.

At this point we note that the Saharan dust particles used in this study are not spherical. For sedimenting particles, shape correction factors, β may be applied to derive the Stokes diameter:

$$D_s = D_a\sqrt{\frac{1}{\rho\beta}} \tag{2}$$

For sedimenting, non spherical quartz particles a shape correction factor of 1.36 has been proposed (Hinds, 1999) which results in a reduction in D_s of ≈15%. However, it is not clear to what extent this correction can be applied to accelerated SDCV particles in the APS. The accuracy of the APS size distribution and number density was tested by measuring these parameters over a prolonged (≈60 min) flow of SDCV through the instrument and weighing the total dust sample. The dust mass was then compared to that calculated mass based on the APS total number of particles in each size bin and the known density of the dust. The results showed that the true mass (weighed) was ≈ a factor 2 (±0.3) greater than that obtained from the APS, which would translate to an underestimate of the average particle size of ≈25%. This value is taken into consideration when we later discuss the experimental data and the calculation of uptake coefficients. In the following text, we cite the Stokes equivalent diameter, D_s. without correction for particle shape.

We note that the SDCV particle size of close to 1 μm measured here is similar to measurements of Saharan dust in the atmosphere, which indicate effective diameters of 1.2–6 μm (Immler and Schrems, 2003), or average values of 1.7 μm (Meskhidze et al., 2005).

2.2 Knudsen reactor

2.2.1 Reactor parameters

The Knudsen reactor-mass spectrometer was used in an essentially identical manner as previously reported (Hanisch and Crowley, 2001b). The pressure in the 296±2 K, Teflon coated Knudsen cell was varied between 0.08 and 0.13 mTorr with the concentration of N_2O_5 varied between 3×10^9 and 2×10^{10} molecule cm^3. In the present experiments, only the

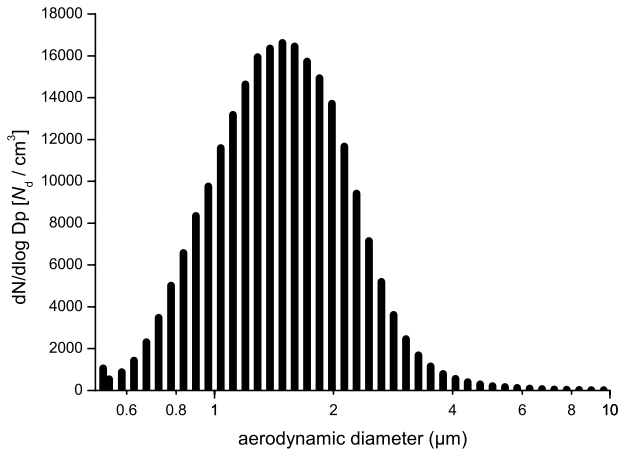

Fig. 2. Size distribution of SDCV as measured by the aerodynamic particle sizer spectrometer. Note that no particles were observed out to 17 μm, the end of the APS measurement range.

10.0 mm escape orifice was used. The mineral samples were prepared by mixing into a paste with methanol and dispersed to form even films on polished α-Al_2O_3 (1120) crystals, which were shown to have no observable reactivity towards N_2O_5. The films, of geometric surface area 1.0 cm^2, were heated to 400 K for 5 h under vacuum before allowing to cool to room temperature for an experiment. Alternatively, they were allowed to dry in the sample compartment at room temperature under vacuum for 8 h. The mass of the dust on the α-Al_2O_3 crystal was obtained by weighing after the experiment.

Gas phase N_2O_5 was introduced into the reactor in a small flow of dried N_2 passed over N_2O_5-crystals held in a vessel at temperatures of between 208 and 203 K. The N_2O_5 concentration, typically $<1\times10^{10}$ molecule cm^{-3}, was calculated assuming saturation of the gas flowing over the N_2O_5.

N_2O_5 was monitored by the NO_2^+ fragment at m/z=46. It was therefore important to establish that HNO_3 impurity was reduced as far as possible, as HNO_3 also fragments to m/z=46. For this reason, the HNO_3 parent ion at m/z=63 was also recorded enabling correction of N_2O_5 concentrations. As the HNO_3 concentration (obtained by comparison with calibration mixtures of HNO_3) (Hanisch and Crowley, 2001b) was <5% that of N_2O_5, this correction was small and had no significant impact on measurements of the uptake coefficient.

2.3 Chemicals/dust samples

N_2O_5 was prepared by mixing dried flows of NO_2 (99.5%) and O_3 in O_2 at room temperature and trapping the product in a cold finger held at 195 K. The reaction time was kept at ≈1 min, which, combined with large O_3 concentrations ensured that all NO_2 was oxidised. This was checked by visually inspecting the complete disappearance of the brown

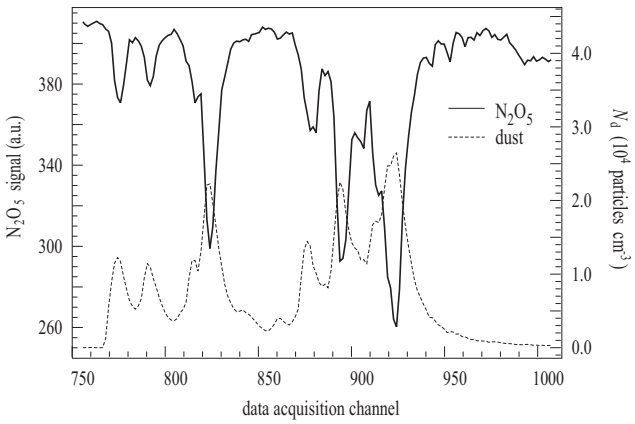

Fig. 3. Response of N_2O_5 (solid line, left y-axis) to the addition of a mineral dust pulse (dotted line, right y-axis) to the flow reactor. The time between acquisition of neighbouring data points was ≈1.7 s.

colour of NO_2 gas within a few seconds of mixing. At the prevailing concentrations, neither O_2 nor O_3 condense at 195 K, so that only N_2O_5 crystals should be present in the trap. The N_2O_5 crystals were stored at 223 K in a darkened vessel. The major impurity was found by mass spectrometry to be HNO_3, which arises via reaction of N_2O_5 with surface bound water.

O_3 was prepared by passing O_2 (Westfalen, 5.0) through a commercial ozoniser, NO_2 (Aldrich, >99.5%) was used as provided. Anhydrous HNO_3 was generated by slowly mixing KNO_3 and H_2SO_4 at 273 K and trapping the HNO_3 vapour at 77 K. Liquid samples of pure HNO_3 were stored in darkened glass fingers at 233 K. N_2 used for the main experimental flow Westfalen 5.0) was used as provided.

The Saharan dust used in these experiments (kindly provided by Laurent Gomes) originates from the Cape Verde Islands (SDCV). Its mineralogy is similar to that described by (Chester and Johnson (1971), its composition, as determined by energy dispersive X-ray spectroscopy, was reported previously (Hanisch and Crowley, 2003b). The Arizona test dust used was a commercial source (Powder technology Inc. MN, USA) of ground Arizona desert sand.

Calcite ($CaCO_3$) is an important component that is present in mineral dust at varying concentrations. The northern part of the Sahara is a region enriched by carbonate soils (Gomes and Gillette, 1993) and Saharan dust consists of 5–30% calcite (Loyë-Pilot et al., 1986; Levin et al., 1990). Desert particles from China contain $CaCO_3$ with a weight fraction of 10–20% (Okada et al., 1987; Matsuki et al., 2005). Our synthetic $CaCO_3$ samples were provided by Aldrich-Sigma.

3 Results and discussion

3.1 Aerosol flow tube experiments

The aerosol flow tube was primarily used to examine the uptake of N_2O_5 to entrained mineral dust samples, the procedures and data analysis are described in Sect. 3.1.1. A small set of experiments were also carried out in the absence of aerosol to establish the reactivity of N_2O_5 at the reactor wall and to determine the diffusion coefficient of N_2O_5 in N_2 (Sect. 3.1.2).

3.1.1 Uptake of N_2O_5 to airborne mineral dust

Despite efforts to provide a stable supply of aerosol to the reactor, the measured particle density showed large fluctuations on a timescale of a few seconds. For this reason, the experiments were always conducted using short bursts (100 s of seconds) of dust into the reactor to observe the response of N_2O_5. A typical data set is displayed in Fig. 3. The striking anti-correlation between the N_2O_5 signal (initial concentration was 5×10^{12} molecule cm^{-3}), with small variations of N_d (number of dust particles cm^{-3}) shows that N_2O_5 is taken up to the dust surface.

In this plot, the dust number density is derived from the analogue output of the APS, and is measured with the same time step (integration time) as the N_2O_5 signal. Due to transport from the reactor to the CLD the signal due to N_2O_5 is shifted ≈1 s later than the dust measurement. This time delay has been corrected in Fig. 3 and for all data sets.

The change of concentration ($[c]$) of a trace gas due to uptake to a surface is given by:

$$k_{\text{obs}} = \frac{d[c]}{dt \cdot [c]} = \frac{\gamma \cdot \bar{c}}{4} \cdot \frac{a}{V} \tag{3}$$

where a is the surface area (cm^2), V is the volume (cm^3) and $\bar{c}$ is the mean molecular velocity (cm s^{-1}) of the trace gas at the appropriate temperature.

Following integration of Eq. (3) the uptake of N_2O_5 to uniformly dispersed dust aerosol under pseudo-first order conditions (number of reactive surface sites not significantly changed during reaction time) may be described by:

$$-\ln\left(\frac{[N_2O_5]_t}{[N_2O_5]_0}\right) = k_d t + k_w t \tag{4}$$

where k_d is the pseudo first order rate coefficient for uptake to dust aerosol (s^{-1}) and k_w is the wall loss rate coefficient (s^{-1}). k_d is thus the gas collision frequency with the dust multiplied by the efficiency of uptake on a per-collision basis, the uptake coefficient, γ:

$$k_d = \frac{\gamma \cdot \bar{c} \cdot A}{4} \tag{5}$$

where A is equal to a/V and is the surface area of the dust aerosol per volume of gas (cm^2 cm^{-3}). The total dust area

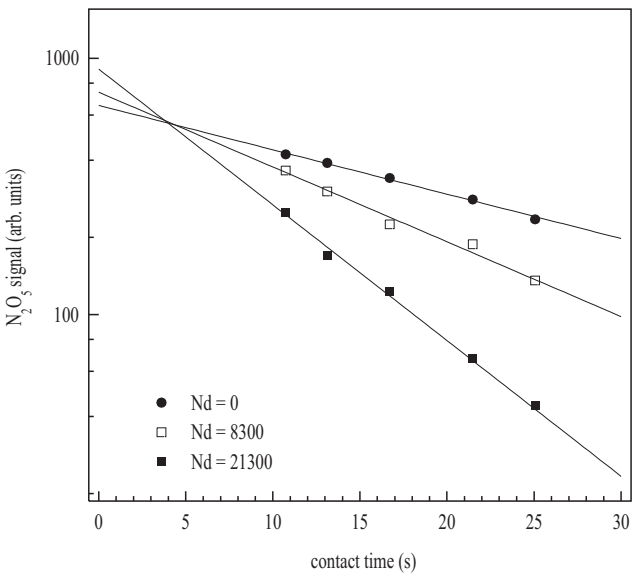

Fig. 4. N_2O_5 signal versus contact time for three dust concentrations. N_d is the number of dust particles per cm^3. The decay of N_2O_5 in the absence of aerosol (N_d=0) is due to loss to the reactor wall. Experimentally determined pseudo first-order loss coefficients were: $(4.0\pm0.3)\times10^{-2}$, $(6.7\pm1.0)\times10^{-2}$ and $(12.2\pm1.6)\times10^{-2}$ for N_d=0, 8300 and 21 300 cm^{-3}, respectively. The errors quoted are 2σ statistical.

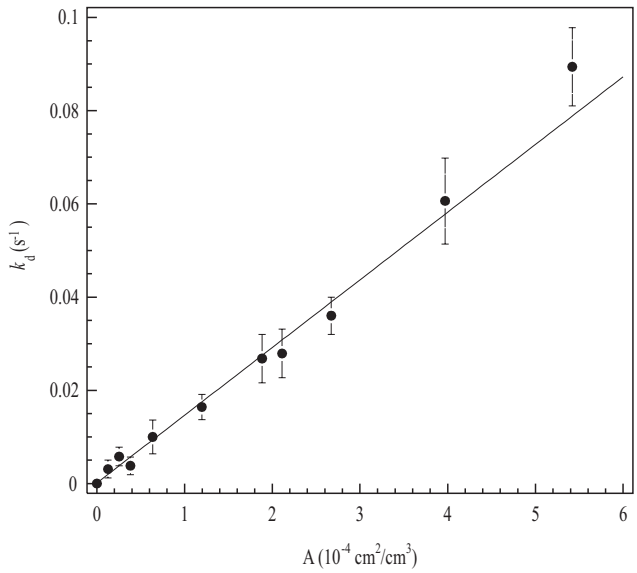

Fig. 5. Dependence of the pseudo first-order decay rate (k_d) of N_2O_5 on the dust surface area. The error bars are 1σ as obtained from unweighted fitting to data sets similar to those shown in Fig. 4.

A, is equal to the product of the number of dust particles per volume N_d (cm^{-3}) and the average surface area of a single dust particle A_d, so that:

$$k_d = \frac{\gamma \cdot \bar{c} \cdot N_d \cdot A_d}{4} \tag{6}$$

k_d is usually derived by combining Eqs. (4) and (5) and plotting the natural log of the relative N_2O_5 concentration versus contact time for a series of dust concentrations as shown in Fig. 4. This analysis requires that the sensitivity of the detector to N_2O_5 remains constant as the experiment progresses. This was generally the case, although sometimes a slight loss (<10%) of sensitivity was observed after a dust burst. A correction to the N_2O_5 signal was applied to take this into account, and was derived by occasionally taking N_2O_5 signals at the same injector position in the absence of dust.

The expected exponential dependence of $[N_2O_5]$ is observed, enabling extraction of k_d. The common intercept of the three data sets shown at $t\approx5$ s is due to finite mixing times and entrance lengths to acquire laminar flow (see Experimental section). The observed pseudo first-order decay constants (k_{obs}) obtained in the presence of dust were corrected by subtracting the separately measured wall loss rate of (4×10^{-2} s^{-1}) and for axial diffusion (Brown, 1978) to obtain k_d. The present flow conditions and loss rates resulted in corrections for axial diffusion of less than 10%. We note that as the loss rate of N_2O_5 to the wall was close to being diffusion limited in these experiments the value of k_w depended strongly on pressure, and only weakly on the state of the wall. Within experimental uncertainty, k_w was thus constant with time and dust concentration. This unusual mode of operation with highly reactive walls can be preferential to one in which the rate of uptake of N_2O_5 to the wall varies with time due to progressive activation of the wall during an experiment to the take up of dust, which, for SDCV could not be avoided. The large (but constant) wall loss rates must however be less than the rate of uptake to aerosol, which was achieved in the present experiments by using large aerosol surface areas.

By plotting k_d versus the dust surface area, A, we can derive the uptake coefficient (Eq. 5) as shown in Fig. 5. The dust surface area was obtained from the experimentally determined number density and size distribution which indicated an average (Stokes) particle diameter of D_s=0.9 μm for this set of experiments and thus an average particle surface area of 2.54×10^{-8} cm^2. The size distribution did not change significantly over the course of an experiment. The error introduced into the dust area calculation by taking the average particle diameter, rather than summed surface area over all size bins was found to be less than 10% (underestimation) due to the symmetric and relatively narrow distribution. Weighted fitting (Eq. 5) to data in Fig. 5 results in a value of $\gamma_{expt}=(2.3\pm0.3)\times10^{-2}$.

The rate of uptake of a trace gas to airborne particles can be reduced by concentration gradients close to the particle surface leading to an underestimation of the true uptake coefficient, γ_{true}. Generally this effect can be corrected (Fuchs and Sutugin, 1970) using:

$$\frac{1}{\gamma_{true}} = \frac{1}{\gamma_{exp\,t}} - \frac{0.75 + 0.283Kn}{Kn\,(Kn+1))} \tag{7}$$

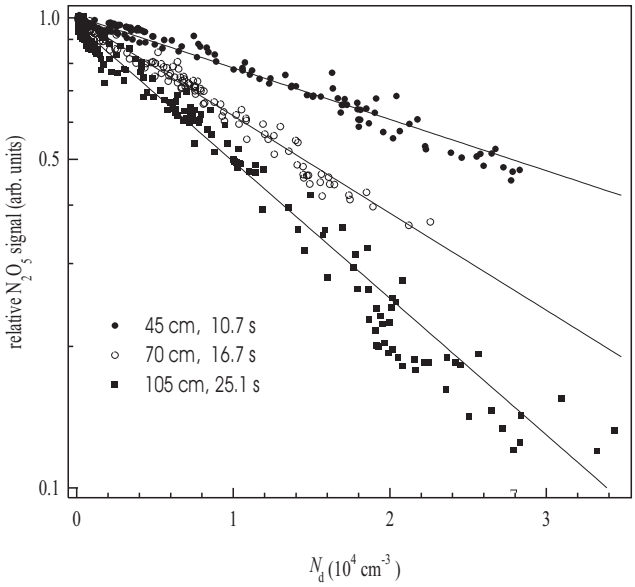

Fig. 6. Dependence of the N_2O_5 signal on the dust concentration at three different injector positions. The slope of the exponential fits (solid lines) is equal to $1/4\gamma\bar{c}A_d t$. The statistical errors on each single data points are within the symbol size.

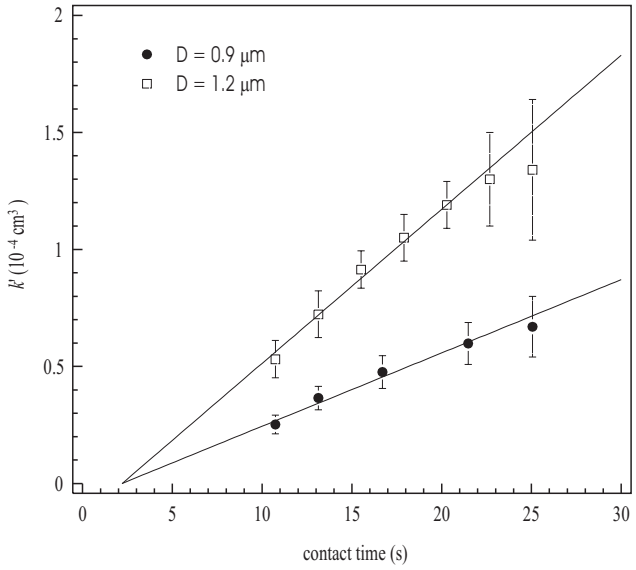

Fig. 7. The slope of the exponential fits to data as shown in Fig. 6 versus contact time for experiments using two different average diameter particle ensembles. The slope, equal to $1/4\gamma\bar{c}A_d$, can be used to derive γ if the particle diameter (and thus A_d) is known.

where $Kn=\frac{3D_g}{\bar{c}\cdot r_{sw}}$, D_g is the gas phase diffusion coefficient of N_2O_5 at atmospheric pressure and 296 K (0.085 cm^2 s^{-1}, see below) and r_{sw} is the radius of the particle at the maximum of the surface area weighted size distribution. The size of the correction is small (≈10%), so that the final value obtained is $\gamma_{\text{true}}=(2.5\pm0.3)\times10^{-2}$. A more exact analysis, in which the diffusion correction was individually applied to each size bin of the distribution shown in Fig. 2, was carried out for one dataset and resulted in an almost identical correction factor (≈11%).

This mode of analysis required using data with roughly fixed dust surface areas (A constant to better than 5%) from datasets similar to those in Fig. 3, in which the dust was not held constant over a long period of time. Indeed, in such experiments the injector was held fixed whilst the dust concentration was varied, making the task of extracting data with the same value of A but at various injector positions somewhat laborious, and which resulted in non-usage of most of the dataset.

Equations (4) and (5) show that, at any fixed contact time, the relative N_2O_5 concentration should display an exponential dependence on the dust number density (N_d). The N_2O_5 signal taken directly before each dust pulse was assigned to $[N_2O_5]_0$ and signals taken continuously during the dust pulse to $[N_2O_5]_t$. By taking a new value of $[N_2O_5]_0$ at each injector position, the wall loss of N_2O_5 was automatically removed from the dataset. With this method, the complete dataset from each "dust pulse" at each injector position can be used. Such a dataset is displayed in Fig. 6. The expected dependence of the N_2O_5 signal on the dust concentration is observed, the slope is equal to $1/4\gamma\bar{c}A_d t$. As the N_2O_5 signal was normalised to the initial signal (before dust was introduced), the intercept does not vary with injector position (contact time) as Eq. (3) suggests. For the particular data set displayed in Fig. 6, data were obtained at a total of 5 contact times, t, corresponding to injector positions of 35, 45, 79, 90 and 105 cm. A plot of $1/4\gamma\bar{c}A_d t$ versus t is given in Fig. 7 for this data set, and for one further dataset obtained using slightly larger particles (1.2 instead of 0.9 μm). As expected from Eqs. (4) and (5) the slope of this plot is dependent on the aerosol diameter, and should be equal to $1/4\gamma\bar{c}A_d$. As described above, the fact that the term $1/4\gamma\bar{c}A_d t$ does not go though zero at t=0 is related to an offset in the contact time due to mixing effects. This does however not affect the analysis, which relies on the slope to derive γ.

Once corrected using Eq. (7), this analysis yields a value for the uptake coefficient of $(2.2\pm0.1)\times10^{-2}$, for the same data set used above to obtain $(2.5\pm0.3)\times10^{-2}$ using the more conventional analysis, and is also in agreement with the value of $(2.7\pm0.4)\times10^{-2}$ derived from the data set displayed in Fig. 7 using larger particles. The good agreement suggests that the approach is sound, and the slight difference in the value of γ obtained when using the conventional versus complete analysis is related to the use of different sections of the same dataset. Thus, although the second approach has the advantage that the complete data set can be analysed, it suffers from the disadvantage that the axial diffusion correction (Brown, 1978) is not easy to apply. However, the axial diffusion correction was only 10% under the flow conditions of

this study, this is considered negligible compared to errors in the particle surface area (see below).

We note that operating the AFT in "pulsed" mode may result in axial gradients in dust number density, the severity of which depend on the relationship between pulse duration and the flow tube residence time. Axial concentration gradients are not taken care of in the simple steady state analysis used here and may give rise to systematic error. In fact, although there is clear anticorrelation between the dust number density and the N_2O_5 concentration, close examination shows that the widths of corresponding features in the dust number density and the N_2O_5 concentration are not identical. However, there is no significant and systematic deviation from the expected exponential dependence of the N_2O_5 concentration on dust number density even in datasets in which numerous dust features of variable duration (see e.g. Fig. 6) were observed. Although some of the experimental scatter in such datasets may arise because of partial break down of the steady state analysis, this is not the major source of error in these experiments, but might lead to a slight underestimation of the uptake coeffcient.

In total, 20 experiments were carried out using 3 different initial N_2O_5 concentrations and 4 different particle diameters. In 12 experiments the gas flow was not humidified (RH≈0), in 4 experiments RH was set to 29% and in 4 it was set to 58%. All values of γ_{true} obtained are summarised in Table 1. The errors associated with γ_{true} in the table are derived as described above from a propagation of statistical errors (2σ) in analysing the datasets. The corrections for axial and radial diffusion and for gas transport to the particles (Eq. 7) were only of the order of 10% and errors associated with these corrections are not considered. The error in the particle concentrations are represented by the scatter of the data points in the plot of Fig. 6 and are thus taken care of in the statistical 2σ error. Taking a critical look at our data, the most obvious source of systematic error arises from the surface areas used to calculate γ. We have calculated the total dust surface area from the average particle diameter from the size distribution and the total number of particles, which results in an underestimation by ≈10%. As discussed in the experimental section, a more serious error is related to the conversion of the measured aerodynamic particle diameter to a geometric one, bearing in mind that the particles are non spherical. The effect of irregular particles on the aerodynamic diameter as measured by the APS is difficult to assess, and has been reported to be potentially as large as a factor of two (Hinds, 1999). Our measurements of time-integrated particle mass indicated that the APS may underestimate this parameter by a factor of two, which converts to underestimation of the average diameter by a factor 1.25, or the surface area by a factor of ≈1.6. In addition, for a given mass, the ratio of surface area of non-spherical to spherical particles varies from 1.24 for a cube, 1.39 for elongated particles with ratio of long to short axis of 3, to a value of ≈1.5 for a plate shaped particle with the ratio of diameter to depth of 8. These considerations lead us to correct our uptake coefficients by a factor of 1.6±0.2 obtained from the measurements of integrated particle mass. The values of γ_{true} listed in Table 1 already take this into account. Experimental scatter (probably arising as a result of fluctuations in detector sensitivity during the experiment) is sufficiently large so that a weak dependence in the uptake coefficient on $[N_2O_5]$ or particle size would remain undetected. The weighted mean values of γ_{true} of $(1.3\pm0.2)\times10^{-2}$, $(0.8\pm0.2)\times10^{-2}$, and $(0.5\pm0.1)\times10^{-2}$ obtained at relative humidities of 0%, 29% and 58%, respectively may indicate some apparent trend, with the lower values obtained at higher relative humidities. Potential reasons for this unexpected trend are discussed later.

A further potential source of error in our measurements is the fact that N_2O_5 is accompanied by the products of its thermal dissociation, NO_2 and NO_3, which are in dynamic equilibrium. Any process (e.g. uptake to dust) that removes N_2O_5 from the reactor will result in an adjustment of the equilibrium concentrations of NO_3 and NO_2 and reformation of N_2O_5 via Reaction (R2). The extent of this effect was tested by numerical simulation (Curtis and Sweetenham, 1987). The simulation

Table 1. Aerosol flow tube experiments: Uptake coefficients and experimental conditions.

RH (%)	$[N_2O_5]$[a]	D_s (μm)	γ_{true} (10^{-2})	γ_{true} (mean)[b] (10^{-2})
0	5	0.9	1.5±0.3	
0	5	0.9	1.4±0.3	
0	6	0.9	1.7±0.4	
0	20	0.9	1.2±0.2	
0	5	0.9	1.4±0.3	
0	5	1.2	1.7±0.4	
0	5	1.2	1.7±0.4	1.3±0.2
0	5	0.8	2.0±0.4	
0	5	0.9	2.0±0.4	
0	5	0.7	0.9±0.2	
0	5	0.8	1.5±0.4	
0	5	0.7	0.9±0.2	
29	5	0.9	1.1±0.2	
29	5	0.9	0.9±0.2	0.8±0.2
29	5	0.9	0.9±0.2	
29	20	0.9	0.6±0.1	
58	5	0.7	0.4±0.1	
58	5	0.7	0.7±0.2	0.5±0.1
58	5	0.7	0.4±0.1	
58	5	0.8	0.7±0.2	

[a] Units of 10^{12} molecule cm^{-3}. γ_{true} has been corrected for systematic errors due to diffusion limitation to the uptake and also for errors in measurement of the particle size/shape (see text for details).
[b] Weighted average.

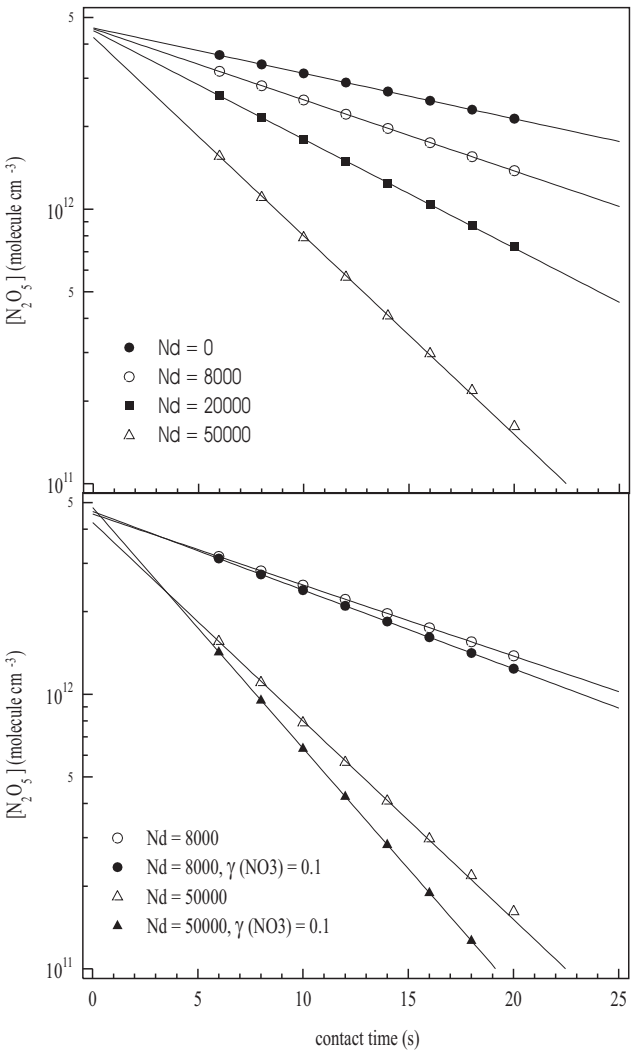

Fig. 8. Simulated N_2O_5 profiles, for details see text. Upper panel: Effect of $N_2O_5 \Leftrightarrow NO_2+NO_3$ equilibrium on the uptake kinetics of N_2O_5. N_d is the dust particle number density (cm^{-3}). Lower panel: Effect of NO_3 uptake to dust (assuming $\gamma(NO_3)$=0.1) on the N_2O_5 profiles. The open symbols are simulations without loss of NO_3, the closed symbols represent the effect of γNO_3=0.1 with two different dust concentrations.

was initialised with $[N_2O_5]=5\times10^{12}$ molecule cm^{-3} with NO_3 and NO_2 at their equilibrium concentration at 296 K (2.7×10^{11} molecule cm^{-3}). Further input parameters were $\gamma_{true}=2\times10^{-2}$ and the particle number density (0, 8000 or 20 000 cm^{-3}) and diameter (0.9 μm) and a first order loss rate coefficient of 0.04 s^{-1} to simulate wall loss. The kinetic parameters for (R2) and (R-2) (the only purely gas phase reactions involved) were taken from an evaluation (Sander et al., 2006).

These parameters were chosen to mimic the real data shown in Fig. 4. The value of γ_{true} was converted in the simulation to a pseudo first-order uptake coefficient using Eqs. (6) and (7). The results of the simulation are shown in Fig. 8 (upper panel). The simulated profiles (symbols) were fitted to an exponential function to derive the total first order loss coefficient (k_{obs}) as carried out for the real experimental data. The results showed that the fitted values of k_{obs} underestimated the input parameters (k_w+k_d) by 5–10%, which is attributed to the regeneration of N_2O_5 as described above. This effect can be considered negligible compared to uncertainty in the particle surface area. Close inspection of the simulated data sets (especially at high loss rates for e.g. 50 000 particles cm^{-3}) showed slight deviation from exponential behaviour for exactly this reason. This would not be detectable in real experimental data with associated noise.

Further, we investigated the impact of the uptake of NO_3 to dust, which, via equilibria (R2) and (R-2), could conceivably also change the N_2O_5 concentration. A large uptake coefficient for reaction of NO_3 with Saharan dust of $\gamma(NO_3)\approx0.1$ was recently reported (Karagulian and Rossi, 2005) and we have used this value in our simulation, the results of which are displayed in Fig. 8 (lower panel). The addition of a loss process for NO_3 has the expected result of enhancing the N_2O_5 loss rate, though the N_2O_5 decay remains exponential. The effect on k_{obs} is however not large ($\approx$10%). Simulations with larger values of $\gamma(NO_3)$ do not significantly change this picture as under the present experimental conditions diffusion limitation for uptake to the particles becomes large. The addition of a wall loss for NO_3 at approximately twice the rate of N_2O_5 wall loss had minimal effect when compared to its uptake to aerosol. In summary, the fact that N_2O_5 is not introduced into our reactor as a pure substance but in equilibrium with NO_3 and NO_2 at the few percent level does not have a significant effect on our analysis of N_2O_5 uptake.

3.1.2 Diffusion coefficient and wall loss of N_2O_5

A series of experiments, all at a total flow rate of 3 SLM and $[N_2O_5]\approx2\times10^{12}$ molecule cm^{-3}, was carried out to examine the loss of N_2O_5 to the walls of the flow tube, whereby no aerosol was entrained in the gas flow but was present on the inner surface of the flow tube in varying, but not controlled amounts.

From Eq. (3), the uptake of a trace gas to a cylindrical surface ($a=2\pi rl$ and $V=\pi r^2 l$) is given by:

$$k_w = \frac{\gamma \cdot \bar{c}}{4} \cdot \frac{2}{r} \tag{8}$$

where k_w is the pseudo first-order loss rate coefficient for wall loss, and γ is the uptake coefficent for this process. For the case where the rate of loss of gas is determined not by surface reactivity, but by diffusion through the gas-phase, the following expression holds.

$$\gamma_{diff} = \frac{3.66(2D_g)}{\bar{c}r} \tag{9}$$

where D_g is the gas phase diffusion coefficient of N_2O_5 at the experimental pressure. Combining Eqs. (8) and (9), and rearranging we obtain:

$$D_g = \frac{k_w r^2}{3.66} \tag{10}$$

Which is valid for Peclet numbers in excess of ≈20 (Zasypkin et al., 1997). The present experimental conditions resulted in Peclet numbers (Pe=$2rv/D_g$, where v is the average linear velocity of the gas flow) of greater than 100.

By varying the injector position, the pseudo first order loss rate of N_2O_5 to the wall (k_w) could be determined at various pressures and converted to values of D_g via Eq. (10). This analysis is appropriate if the uptake is irreversible over the time scale of the experiments (i.e. N_2O_5 is lost permanently to the wall). For any given injector position, the N_2O_5 signal was seen to be invariant with exposure time, confirming that the capacity of the (dusty) walls to take up N_2O_5 was sufficiently large. Exponential plots of [N_2O_5] versus contact time confirm this (Fig. 9 upper panel). Data were analysed at contact times longer than required for laminar flow to establish (≈3 s at 350 Torr and ≈5 s at 760 Torr).

A linear relationship between k_w and pressure showed that at all experimental pressures covered (350 to 750 Torr) the uptake was indeed limited by gas-phase diffusion.

The results of such an experiment are summarised in Fig. 9 (lower panel) which also plots the values of D_g obtained via Eq. (10) with previous experimental and theoretical data, most of which present diffusion coefficients at 750–760 Torr. The scatter in the dataset (e.g. at 500 Torr) is larger than that resulting from a rigorous statistical analysis of each data point, and may be a result of non-perfect centring of the injector during translation.

The present data set is entirely consistent with the experimental result of Carstens at 760 Torr (Carstens, 1998), obtained using a completely different approach and also with the various calculated values listed (Monchick and Mason, 1961; Fried et al., 1994; Lovejoy and Hanson, 1995; Hu and Abbatt, 1997) at or close to this pressure. The parameterisation of Monchick and Mason (Monchick and Mason, 1961) also reproduces the observed pressure dependence rather closely. The value we obtained at 296 K and 760 Torr, $D_{N_2O_5}$=0.085 cm^2 s^{-1}, was used in the diffusion corrections reported above.

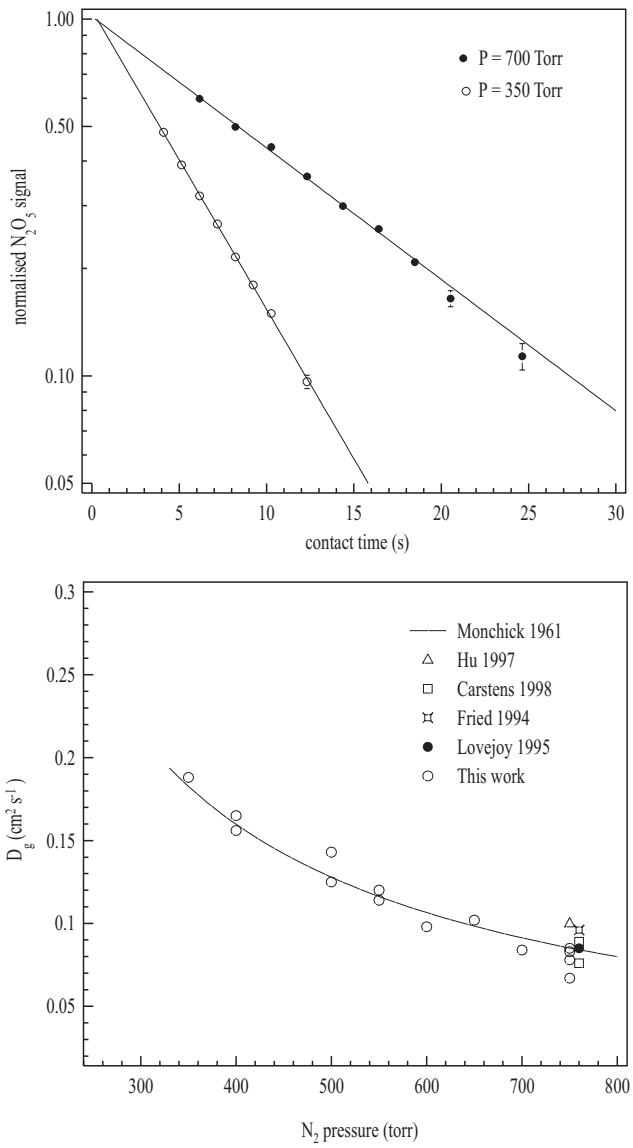

Fig. 9. Upper panel: Exponential decay profiles of N_2O_5 due to loss at the reactor wall at experimental pressures of 350 and 700 Torr. The error bars are derived from propagation of errors in the NO difference signal. Lower Panel: Pressure dependent diffusion coefficients from the present study compared to experimental results (Carstens, 1998) and theoretical calculations: Hu 1997 = Hu and Abbatt (1997), Fried 1994 = Fried et al. (1994), Monchick 1961 = Monchick and Mason (1961), Lovejoy 1995 = Lovejoy and Hanson (1995). For the present data set, statistical errors (from e.g. data sets as shown in the upper panel) were smaller than the symbol size.

3.2 Knudsen reactor experiments

The Knudsen reactor was used to investigate the uptake of N_2O_5 to bulk samples of SDCV, ATD and calcite at 296±2 K. The effect of changing parameters such as the sample mass (i.e. thickness), the N_2O_5 concentration and the heating of the sample under vacuum (drying) were investigated.

3.2.1 SDCV results

Data from an experiment in which a bulk SDCV sample (21.6 mg spread onto the 1 cm^2 sample holder) was exposed to ≈6×10^9 molecule cm^{-3} of N_2O_5 is displayed in Fig. 10.

Once slight drifts (<10% over 30 min) in signal had been removed from the data, correction was made to the raw N_2O_5

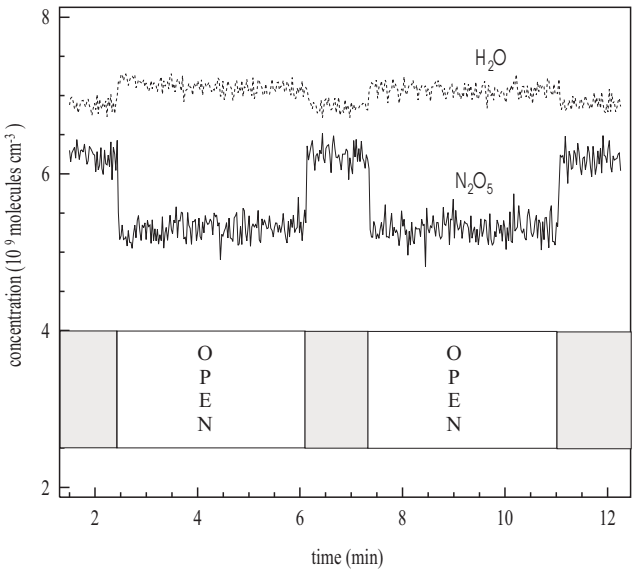

Fig. 10. Knudsen reactor data for the uptake of N_2O_5 to 21.6 mg of SDCV. The release of H_2O from the dust sample upon opening the lid to the sample chamber (multiplied by a factor of 3 for clarity) and the times of opening and closure of the sample chamber (open) are also indicated.

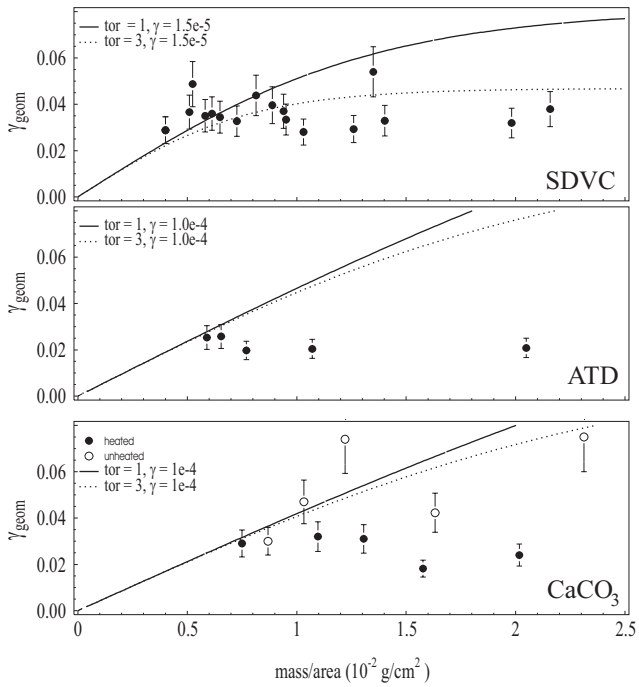

Fig. 11. Uptake coefficients (γ_{geom}) for interaction of N_2O_5 with Saharan dust (SDCV), Arizona test dust (ATD) and calcite. For SDCV and ATD all samples were dried by heating prior to the experiment. For $CaCO_3$ the solid circles indicate uptake coefficients obtained using heated samples. The open circles are data points from unheated samples. The smooth lines represent calculations using a pore diffusion model to take into account the interstitial surface area of the sample. The full line was calculated with a tortuosity factor (tor) of 1, the dashed line with a value of 3 (see text for details).

mass spectrometer signal at m/z=46 to take into account low levels of HNO_3 present in the reactor as evidenced by a weak signal at m/z=63.

The weak signal at m/z=63 was acquired by integrating for much longer than that at m/z=46. As this procedure took several minutes, it was performed before each uptake experiment using the same flow conditions. During non-exposure periods, the m/z=46 signal was corrected using the known fragmentation pattern of pure HNO_3 samples, whereas during exposure the drop in HNO_3 signal was calculated using its uptake coefficient from our previous studies (Hanisch and Crowley, 2001a; Hanisch and Crowley, 2001b), which was then converted to a change in m/z=46 due to HNO_3. The corrections were in fact very small (only a few percent of the signal due to the low concentration of HNO_3) and had only minor influence on values of γ obtained.

During exposure, the N_2O_5 concentration dropped to a steady state value defined by the rate of uptake to the surface and the rates of flow into and escape from the reactor. We have chosen to use a large escape orifice in these experiments in order to avoid concentration gradients at the surface, which can result in the underestimation of the uptake coefficient (see Hanisch and Crowley (2001a, b) for details). Unlike in the AFT experiments, the dust is not replenished during the course of the experiment but can be chemically modified. Due to the low concentrations of N_2O_5 used, no significant change in reactivity over a typical exposure period was observed.

As in our previous experiments on HNO_3 (Hanisch and Crowley, 2001a; Hanisch and Crowley, 2001b) the uptake coefficient was derived by the difference in trace gas signal when the gas flow was either isolated (S_0) or in contact with the dust sample (S_d). It was not necessary to know the N_2O_5 concentration absolutely.

$$\gamma_{\text{geom}} = \frac{k_{\text{esc}}}{\omega}\left(\frac{S_0}{S_d} - 1\right) \tag{11}$$

where γ_{geom} is the uptake coefficient calculated using the geometric surface area of the sample, k_{esc} is the escape rate coefficient ($10.0\,\text{s}^{-1}$) and ω is the collision rate with the sample and was calculated from:

$$\omega = \frac{\bar{c}A_g}{4V} \tag{12}$$

where A_g is the projected, geometric surface area of the dust sample ($1.0\,\text{cm}^2$), $\bar{c}$ is the mean molecular velocity of N_2O_5 at 296 K and V is the volume of the reactor ($120\,\text{cm}^3$). Values of γ_{geom} obtained by this expression are listed in Table 2, where the initial N_2O_5 concentration and the dust mass are

also given. As the N_2O_5 profile during uptake shows no sign of saturation, the initial uptake (γ_0, obtained from the signal drop just after opening the sample holder) is equal to the steady state uptake, γ_{ss}.

The data, plotted in Fig. 11, are encompassed by the value γ_{geom}=(3.7±1.2)×10^{-2}. Three quantities contribute significantly to the total statistical error of ≈10% in these experiments (error bars in Fig. 11): k_{esc} was determined with an accuracy of ≈5%; the error in ω was estimated as ≈5% due to uncertainty in the coverage of the dust on the α-Al_2O_3 crystal, which was observed to contract slightly at the edges during the drying procedure. The error in the signal at m/z=46 is dependent upon the size of the signal since random noise remains fairly constant and contributes ≈5%, the effect of HNO_3 correction is comparably negligible. The scatter found in experiments conducted under "identical" conditions was however considerably larger than 10%, suggesting that experiment-to-experiment deviations in e.g. the morphology of the dust sample are responsible. We note that this analysis assumes that the projected geometric surface area is appropriate for extracting the uptake coefficient from the raw data. As described in detail before, this assumption can be tested by variation of the dust mass to estimate the role of diffusion of N_2O_5 into interstitial space within the bulk sample on the time scale of measurement of the initial signal drop (Keyser et al., 1991; Hanisch and Crowley, 2003b). Using previously reported bulk sample densities (Hanisch and Crowley, 2003b) and average particle diameters for identically prepared SDCV samples, we calculate that variation of the sample mass between 4 and 21 mg is equivalent to variation of the number of layers between (very approximately) 40 and 200. This is similar to the range adopted in our experiments on O_3 uptake to the same SDCV samples (Hanisch and Crowley, 2003b). Thinner samples could not be prepared using our procedure. The dependence of γ_{geom} on the sample mass is illustrated in Fig. 11. In contrast to our experiments with O_3, but similar to our experiments with HNO_3 (Hanisch and Crowley, 2001a; Hanisch and Crowley, 2001b) no dependence on sample mass was found. The data listed in Table 2 also shows no dependence of γ_{geom} on the initial concentration of N_2O_5 (varied over a factor of almost 4). The solid line though the SDCV dataset in Fig. 11 is a predicted dependence of γ_{geom} on sample mass using the pore diffusion correction equations and physical parameters for SDCV from our previous publication (Hanisch and Crowley, 2003b) which are listed along with data for ATD and $CaCO_3$ in Table 3. With the tortuosity factor kept at either 1 or 3 and the average particle diameter found from the AFT experiments (≈0.9 μm), values of γ_{true} of ≈1–2×10^{-5} (i.e. a factor ≈3000 lower than γ_{geom}) was found to reproduce the data adequately. We note however, that the dataset did not sample both the mass independent regime (large masses) and the strongly mass dependent regime at low dust masses, which precludes proper assessment of the applicability of the model and the usual

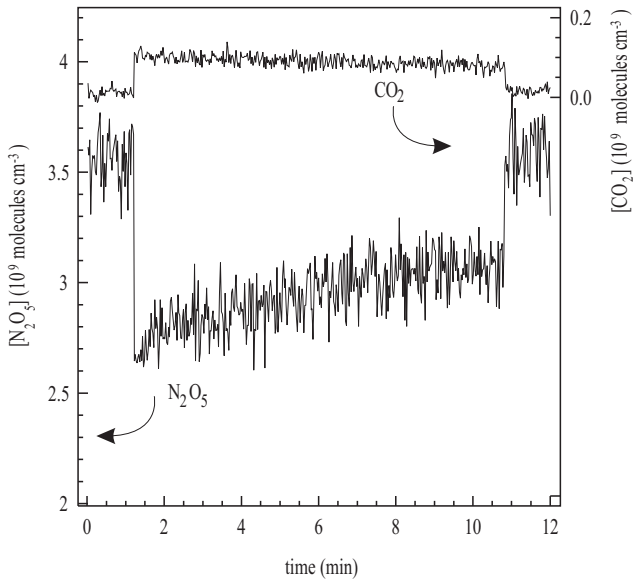

Fig. 12. Uptake of N_2O_5 to an unheated $CaCO_3$ sample. N_2O_5 was measured at m/z=46, CO_2 at m/z=44.

empirical derivation of the tortuosity factor. The choice of tortuosity factor of 1 or 3 was guided by the study of Boulter and Marschall (Boulter and Marschall, 2006), who suggest that values in excess of 3 are unlikely. Moreover, we note that the pore diffusion analysis requires knowledge of the average grain size, which ideally should be characterised by a narrow size distibution. Inspection of SEM pictures of our SDCV sample revealed a very wide range of sizes (<0.3 μm to >10 μm) and it is unclear whether an average grain diameter based on the APS size is applicable. The application of the pore diffusion model to inhomogeneous, bulk samples is precarious and a more detailed analysis is, in this case, not warranted.

As shown in Fig. 10, during opening of the sample holder we also monitored H_2O at m/z=17 (OH^+) and always observed some release of H_2O from the sample (this effect was seen when no N_2O_5 was present) showing that some residual moisture resided in the bulk sample. No correlation was observed between the amount of water desorbing (a measure of the "dryness" of the sample) and the uptake coefficient. Products such as CO_2 or HNO_3 were not observed in these experiments.

3.2.2 Arizona test dust

Uptake coefficients for N_2O_5 on ATD were measured at five different sample masses and concentrations between 3.3 and 11×10^9 molecule cm^{-3}. The data was qualitatively similar to that observed for SDCV, i.e. time independence of the signal during exposure and the treatment was identical.

The uptake coefficients are listed in Table 2 and plotted versus sample mass in Fig. 11. As for SDCV there is no significant dependence of the uptake coefficient on

Table 2. Uptake coefficients and conditions for Knudsen reactor experiments.

SDCV			ATD			$CaCO_3$		
$[N_2O_5]^a$	mass[b]	γ^c	$[N_2O_5]^a$	mass[b]	γ^c	$[N_2O_5]^a$	mass[b]	γ^e
11.0	9.4	3.7±0.7	10.4	10.7	2.0±0.4	4.1	13.1	3.1±0.5
6.6	12.6	2.9±0.6	6.8	20.5	2.1±0.4	4.5	7.5	2.9±0.5
5.2	19.8	3.2±0.6	4.1	6.5	2.6±0.5	3.4	32.0	2.0±0.4
4.7	8.9	4.0±0.8	3.3	5.9	2.5±0.5	2.7	15.8	1.8±0.4
4.9	5.8	3.5±0.7	3.5	7.7	2.0±0.4	2.9	11.0	3.2±0.4
3.0	6.1	3.6±0.7				3.4	20.2	2.4±0.5
3.6	6.5	3.4±0.7				3.3	12.2	7.4±1.5*
3.6	9.5	3.3±0.7				3.6	23.1	7.5±1.4*
6.0	5.1	3.7±0.7				3.1	10.3	4.7±1.0*
6.3	21.6	3.8±0.8				2.2	16.3	4.2±1.0*
5.1	14.0	3.3±0.7				1.7	9.0	3.0±0.7*
5.1	10.3	2.8±0.6						
3.6	7.3	3.3±0.7						
4.1	5.2	4.9±1.0						
3.9	8.1	4.3±0.9						
5.8	4.0	2.9±1.0[d]						

All experiments were conducted at 296±2 K.
[a] Concentrations in 10^9 molecule cm^3.
[b] Mass of sample per cm^2.
[c] γ ($\times 10^{-2}$) is reported for heated samples, unless denoted with a star (unheated).
[d] Obtained using the 2.25 cm^2 sample holder.
[e] γ ($\times 10^{-2}$) is the initial uptake coefficient.

Table 3. Physical charactierstics of the bulk dust samples used in pore diffusion calculations.

	Dust Type		
Parameter ↓	SDCV	ATD	$CaCO_3$
BET surface area (m^2/g)	39.6	5.7	5.1
particle density (g/cm^3)	2.7	2.65	2.93
sample density (g/cm^3)	1.2	1	1
diameter (μm)	1	5[a]	5[a]

[a] Estimated from SEM pictures of the sample.

sample mass or N_2O_5 concentration, with an average value of γ_{geom}=(2.2±0.8)×10^{-2}. The larger average particle diameter means that at 5 mg sample mass, only about 10 formal layers of height 5 μm are present. Under such conditions, the calculations for the pore diffusion analysis suggest that, due to the larger particles and lower BET surface areas, the linear mass dependent regime should extend beyond 15 mg cm^{-2}. The pore diffusion calculations were initiated with tortuosity factors of 1 or 3 as for SDCV. Clearly, the predicted dependence of γ_{geom} on sample mass is not observed in the dataset, suggesting that the N_2O_5 is not interacting significantly with internal surface area of the bulk sample. In order to align the model prediction with the dataset, an unrealistically large value for the tortuosity factors (≈50) is required, implying that application of the pore diffusion model is inappropriate, and that (on the time scale of our experiments) reaction takes place mainly at the surface layer. We note that the use of the projected geometric surface area must however result in a value of the uptake coefficient that is an upper limit as, even in the absence of diffusion into the bulk sample, surface roughness is neglected. This may result in surface area enhancements of a factor of two or more, depending on the sample morphology and the grain size. As for SDCV, no significant release of CO_2 could be observed.

3.2.3 Calcite ($CaCO_3$)

A total of 11 experiments were conducted with both heated (≈400 K for >5 h) and unheated $CaCO_3$ samples. For the 6 heated samples (Fig. 11) the uptake coefficients were found to be similar to those found for ATD, with an average, mass independent value of the uptake coefficient of (2.6±0.8)×10^{-2}. A number of differences between the unheated and heated samples were observed, including a time dependent N_2O_5 signal during exposure to the unheated samples, with initially large uptake coefficients decreasing over a period of 10 min. An example of a raw data set showing uptake to unheated $CaCO_3$ is given in Fig. 12. For

Table 4. Summary of laboratory studies of N_2O_5 uptake to mineral dust samples at room temperature.

Dust	uptake coefficient (10^{-2})	method/RH	notes	Reference
SDCV	γ_0=8.0±0.3	Knudsen/0 %	a	(Seisel et al., 2005)
	γ_{ss}=1.3±0.3	Knudsen/0%	a	(Seisel et al., 2005)
	γ=0.91±0.07	DRIFTS/0%		(Seisel et al., 2005)
	γ_0=30±8	Knudsen/0%	b	(Karagulian et al., 2006)
	γ_{ss}=20±5	Knudsen/0%	b	(Karagulian et al., 2006)
	γ_0=γ_{ss}=3.7±1.2	Knudsen/0%	c	This work
	γ=1.3±0.2	AFT/0%		This work
	γ=0.8±0.2	AFT/29%		This work
	γ=0.5±0.2	AFT/58%		This work
ATD	γ_0=20±6	Knudsen/0%	b	(Karagulian et al., 2006)
	γ_{ss}=11±3	Knudsen/0%	b	(Karagulian et al., 2006)
	γ_0=γ_{ss}=2.2±0.8	Knudsen/0%	c	This work
$CaCO_3$	γ_0=12±4	Knudsen/0%	b	(Karagulian et al., 2006)
	γ_{ss}=2.1±0.6	Knudsen/0%	b	(Karagulian et al., 2006)
	γ_0=2.6±0.8	Knudsen, heated/0%	c	This work
	γ_0=5±2	Knudsen, unheated/0%	d	This work

[a] Sample generated from aqueous slurry and dried under vacuum *without* heating.
[b] Sample dried at 294 K under vacuum until water desorption ceased.
[c] Sample generated from slurry in methanol and dried under vacuum whilst heating to 450°C.
[d] Sample generated from slurry in methanol and dried under vacuum *without* heating. For all Knudsen reactor experiments the uptake coefficient was derived from the projected, geometric surface area of the bulk sample and are thus upper limits.

this dataset, γ decreased from a value of 7.5×10^{-2} immediately after exposure started to a value of 3.6×10^{-2} after 11 min, ≈ a factor of two smaller. Note that the uptake coefficients listed in Table 2 are the initial (maximum) uptake coefficients.

Concurrent with the loss of N_2O_5 to the surface, we observed formation of CO_2 (measured at m/z=44) which is closely anti-correlated with the N_2O_5 signal. On the time scale of the experiments, the CO_2 is formed promptly. By calibrating the mass spectrometer for both N_2O_5 and CO_2 we were able to calculate that the yield of CO_2 per N_2O_5 lost to the surface was 0.09 (±0.02) for both the heated and unheated samples. This observation is qualitatively similar to previous results from this laboratory describing the interaction of HNO_3 with $CaCO_3$, which also produces CO_2 though at a much higher (≈30%) yield (Hanisch and Crowley, 2001a).

The results of the pore diffusion correction for N_2O_5 uptake to the bulk $CaCO_3$ substrate is ambiguous. Considering only the data obtained with heated samples, we see that, when constrained by reasonable values of the tortuosity, the pore diffusion model cannot reproduce the independence of the uptake coefficient on sample mass. The data obtained using non heated samples displays higher values of the initial uptake coefficient with some apparent dependence on the sample mass, but also significantly more scatter which, in combination with a limited set of data, precludes an accurate pore diffusion analysis.

4 Summary – comparison with literature and atmospheric implications

The complete dataset from this study is compiled with previous literature determinations (Seisel et al., 2005; Karagulian et al., 2006) of uptake coefficients in Table 4. Values of the initial uptake coefficient (i.e. to a fresh surface) and a steady state uptake coefficient are noted, the Knudsen reactor experiments, both in the present study and in the literature used the geometric surface area to derive the uptake coefficient so that direct comparison should, in principle, be possible.

The most comprehensive dataset is for SDCV, for which Knudsen reactor derived initial uptake coefficients vary between $\approx4\times10^{-2}$ and 30×10^{-2} with some of this variability likely to be due to different methods of sample preparation as indicated in Table 4. Our Knudsen reactor result appears to be more consistent with the values reported by Seisel et al. (2005) rather than with Karagulian et al. (2006) who report significantly larger values for both initial and steady state uptake coefficients. This is surprising as Karagulian used the very same dust sample as we have. If the gas phase conditions were similar, the discrepancy can only be resolved by assuming significant changes in reactivity induced during sample preparation and sample presentation, or the presence of reactive species in the N_2O_5 flow. Though not mentioned in their manuscript, the samples of Karagulian et al. (2006) were "de-humidified" by evacuation at 294 K for ≈30 min, or until H_2O desorption stopped (F. Karagulian and M. J. Rossi,

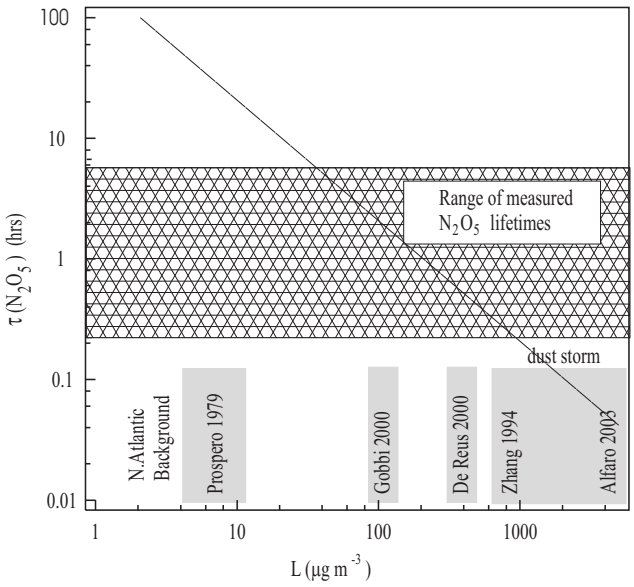

Fig. 13. N_2O_5 lifetime versus dust loading. The smooth line is the lifetime with respect to uptake to mineral aerosol based on the uptake coefficient measured in this work. Illustrative measurements of dust loadings (refs) and N_2O_5 lifetimes are also given. References are: Prospero 1979 = (Prospero, 1979) Gobbi 2000 = (Gobbi et al., 2000) De Reus 2000 = (Reus et al., 2000) Zhang 1994 = (Zhang et al., 1994) Alfaro 2003 = (Alfaro et al., 2003). The literature source of the N_2O_5 lifetimes is given in the text.

personal communication, 2007). This procedure will leave more moisture associated with the bulk substrate than the heating/evacuating procedure adopted in the present study, and may contribute to the discrepancy in the values of γ observed.

A similar picture emerges when the $CaCO_3$ and ATD data of the same two groups are compared, with the uptake coefficients of Karagulian et al. (2006) significantly larger in all cases. Karagulian et al. (2006) observed a dependence of the uptake coefficient on N_2O_5 concentration, with larger values of γ associated with lower concentrations. As our concentrations were significantly lower ($\approx$ factor 100) than those used by Karagulian et al. (2006) this clearly cannot explain the discrepancy observed. A further difference in the two studies is the use of much larger sample masses by Karagulian et al. (2006) (100 and 1800 mg) and the observation of a dependence of γ on sample mass between 0 and 300 mg, which was attributed to incomplete coverage of the sample support. Some of the differences noted above may be attributed to different modes of sample preparation (heating or not-heating during drying), as the non-heated samples from the present study yielded larger values of γ, than the heated samples. Indeed, a factor ≈ 2 difference in γ_0 of Karagulian et al. (2006) and the present study for non-heated samples may be considered to be in reasonable agreement. Qualitative similarities between our Knudsen reactor work and that of Karagulian include the observation of CO_2 release upon exposure of $CaCO_3$ to N_2O_5. The yield of CO_2 reported by Karagulian of 42–50% is however much larger than values of 9% in the present study. Once again the difference is most likely due to sample preparation and the amount of H_2O available for reaction.

As already mentioned, issues related to porosity of the bulk samples can also influence the value of the uptake coefficient obtained from Knudsen reactor experiments. Although all of the studies using Knudsen reactors to investigate N_2O_5 uptake to mineral dust substrates have concluded that pore diffusion is not important, sample surface morphology (roughness) means that the projected geometric area is the minimum area with which collisions are taking place, and that the uptake coefficient so derived are upper limits. Indeed, sample roughness is not a parameter that is easily accessed by the Knudsen studies and will vary from study to study and contribute to scatter in reported values of γ for seemingly identical processes.

Many of the uncertainties related to derivation of uptake coefficients when using porous or grainy bulk substrates in Knudsen reactors are eliminated in the AFT approach, and we consider the uptake coefficients presented for SDCV using the AFT to be more reliable. The agreement in the MPI data sets using both methods is quite satisfactory, yet, given the differences in literature values using Knudsen reactors to investigate this process, may to some extent be fortuitous. For the following discussion of the atmospheric implications of N_2O_5 uptake to mineral dust we consider only the AFT data on SDCV.

Table 1 reveals that, within experimental uncertainty, the measured uptake coefficient for Saharan dust from the AFT experiments is independent of most experimental variables including N_2O_5 concentration. This confirms that the experiments were carried out under conditions in which the number of reactive sites on the dust surface were not significantly depleted during the maximum 30 s exposure to N_2O_5. What is very surprising, however is that the uptake coefficient decreases with increasing relative humidity. As N_2O_5 uptake to surfaces is normally considered to be driven by hydrolysis and the availability of H_2O at the surface, this is counter-intuitive. We note that the uptake coefficient for N_2O_5 to aqueous surfaces has been determined to be close to 0.02 (see references cited by Evans and Jacob, 2005) which is larger by only a factor of $\approx$ two greater than our value obtained at zero humidity, making the existence of a strong RH dependence unlikely. Only for non-reactive uptake do we expect that competitive adsorption with H_2O may reduce the apparent experimental uptake coefficient. As we have no evidence for a reversible component of the N_2O_5 uptake to mineral dust in the presence (or absence) of water this hypothesis remains unsubstantiated. We cannot rule out that the weak negative correlation between the uptake coefficient and RH may arise from an unidentified experimental systematic error, though further (more precise) investigations would to useful to resolve this issue.

The AFT result of a large uptake coefficient at low RH is supported by the Knudsen reactor experiments on SDCV which yield slightly higher uptake coefficients (actually upper limits, see above) at a relative humidity of essentially zero.

The Knudsen reactor results for dry, bulk $CaCO_3$ samples, which showed different reactivity if heated or not during drying under vacuum is also revealing in this respect. Water uptake isotherms for $CaCO_3$ show that, at low RH, very little surface adsorbed H_2O can be detected (Gustafsson et al., 2005) and suggest that the enhanced reactivity when comparing non-heated to heated samples is not due only to surface bound water. Compared to commercial $CaCO_3$, Saharan dust contains a significantly larger amount of strongly bound water which is not removed under vacuum at ambient temperatures. Indeed, for some clay minerals water can contribute more than 10 percent to the overall mass, and this water can only be removed by heating to ≈800 K (Grim, 1953). The independence of γ on the availability of H_2O may thus simply reflect that Saharan dust (and clay minerals in general) is always associated with a large "internal" water content and that the reaction with N_2O_5 is not purely a surface phenomenon. In this vein, and as mentioned above, we note that the uptake coefficient for N_2O_5 to an aqueous surface at temperatures close to 300 K is characterised by an uptake coefficient of close to 2×10^{-2}, not much larger than that observed for "dry" or "humid" SDCV. In the following calculations, we thus assume that the uptake of N_2O_5 to mineral dust in the atmosphere is characterised by a single uptake coefficient, independent of e.g. T or RH.

Neglecting limitations due to diffusive transport, the lifetime of a trace gas (τ, in s) with respect to uptake to an aerosol surface may be calculated using the following expression:

$$\tau = \frac{4}{\gamma \cdot \bar{c} \cdot A} \tag{13}$$

where A is the surface area of aerosol per volume of gas ($cm^2\,cm^{-3}$). As dust aerosol loading (L) is usually presented in $\mu g\,m^{-3}$, we note that, by assuming an average particle diameter of 1 μm and density of 2.7 $g\,cm^{-3}$, 1 $\mu g\,m^{-3}$results in a surface area density of $2.2\times10^{-8}\,cm^2\,cm^{-3}$. Expression (13) then becomes:

$$\tau = \frac{4}{\gamma \cdot \bar{c} \cdot L} \cdot 4.5 \times 10^7 \tag{14}$$

The dependence of the N_2O_5 lifetime ($\tau_{N_2O_5}$) on mineral dust loading is presented in Fig. 13, whereby an uptake coefficient of 1×10^{-2} is used in the calculation. Field measurements of N_2O_5 have revealed a pseudo steady state lifetime (shaded area in Fig. 13) which can vary typically between ≈5 min and 2 h (but sometimes as large as 5 h) and which depends heavily on e.g. available aerosol (Heintz et al., 1996; Martinez et al., 2000; Wood et al., 2005; Aldener et al., 2006). Clearly, background dust loading of e.g. ≈14 $\mu g\,m^{-3}$ in the tropical North Atlantic and ≈4–5 $\mu g\,m^{-3}$ in the Mediterranean and Indian Ocean (Prospero, 1979; Prospero and Nees, 1986) will contribute only insignificantly to N_2O_5 loss rates. At intermediate loadings (50 to 100 $\mu g\,m^{-3}$) mineral dust can represent an important sink for N_2O_5 if e.g. the sulphate loading is low, whereas at loadings above 200 $\mu g\,m^{-3}$, mineral dust can provide sufficient reactive surface to become the dominant sink.

Acknowledgements. We thank L. Gomes for his kind provision of the Saharan dust sample used in this study, and J. Schneider (MPI) for the loan of and assistance with the ELPI. Sections of this study were carried out in part fulfilment of the PhD of CW at the Johannes-Gutenberg University in Mainz. We are grateful for partial funding of this work (Knudsen reactor studies) within the EU project MINATROC (EVK2-1999-00003).

Edited by: J. Thornton

References

Aldener, M., Brown, S. S., Stark, H., Williams, E. J., Lerner, B. M., Kuster, W. C., Goldan, P. D., Quinn, P. K., Bates, T. S., Fehsenfeld, F. C., and Ravishankara, A. R.: Reactivity and loss mechanisms of NO_3 and N_2O_5 in a polluted marine environment: Results from in situ measurements during New England Air Quality Study 2002, J. Geophys. Res., 111, D23S73, doi:10.1029/2006JD007252, 2006.

Alfaro, S. C., Gomes, L., Rajot, J. L., Lafon, S., Gaudichet, A., Chatenet, B., Maille, M., Cautenet, G., Lasserre, F., Cachier, H., and Zhang, X. Y.: Chemical and optical characterization of aerosols measured in spring 2002 at the ACE-Asia supersite, Zhenbeitai, China, J. Geophys. Res., 108, 8461, doi:10.1029/2002JD003214, 2003.

Ansmann, A., Mattis, I., Muller, D., Wandinger, U., Radlach, M., Althausen, D., and Damoah, R.: Ice formation in Saharan dust over central Europe observed with temperature/humidity//aerosol Raman lidar, J. Geophys. Res., 110, D18S12, doi:10.1029/2004JD005000, 2005.

Bauer, S. E., Balkanski, Y., Schulz, M., Hauglustaine, D. A., and Dentener, F.: Global modeling of heterogeneous chemistry on mineral aerosol surfaces: Influence on tropospheric ozone chemistry and comparison to observations, J. Geophys. Res., 109, D02304, doi:10.1029/2003JD003868, 2004.

Bian, H. S. and Zender, C. S.: Mineral dust and global tropospheric chemistry: Relative roles of photolysis and heterogeneous uptake, J. Geophys. Res., 108, 4672, doi:10.1029/2002JD003143, 2003.

Boulter, J. E. and Marschall, J.: Measurement of effective Knudsen diffusion coefficients for powder beds used in heterogeneous uptake experiments, J. Phys. Chem. A, 110, 10 444–10 455, 2006.

Brown, R. L.: Tubular flow reactors with first-order kinetics, J. Res. Nat. Bur. Standards, 83, 1–8, 1978.

Carmichael, G. R., Zhang, Y., Chen, L.-L., Hong, M.-S., and Ueda, H.: Seasonal variation of aerosol composition at Cheju island, Korea, Atmos. Environ., 30, 2407–2416, 1996.

Carstens, T.: Labormessungen kinetischer Parameter zur Beschreibung der Spurengasaufnahme in atmosphphärische Wassertröpfchen, University of Bonn, 1998.

Chartrand, D. J. and McConnell, J. C.: Heterogeneous chemistry and the O_3 budget in the lower mid- latitude stratosphere, J. Atmos. Chem., 35, 109–149, 1999.

Chester, R. and Johnson, L. R.: Atmospheric dusts collected off West African coast, Nature, 229, 105–107, 1971.

Curtis, A. R. and Sweetenham, W. P.: Facsimile, AERE, Report R-12805, 1987.

Dentener, F. J., Carmichael, G. R., Zhang, Y., Lelieveld, J., and Crutzen, P. J.: Role of mineral aerosol as a reactive surface in the global troposphere, J. Geophys. Res., 101, 22 869–22 889, 1996.

Dentener, F. J. and Crutzen, P. J.: Reaction of N_2O_5 on tropospheric aerosols – Impact on the global distributions of NOx, O_3, and OH, J. Geophys. Res., 98, 7149–7163, 1993.

Evans, M. J. and Jacob, D. J.: Impact of new laboratory studies of N_2O_5 hydrolysis on global model budgets of tropospheric nitrogen oxides, ozone, and OH, Geophys. Res. Lett., 32, L09813, doi:10.1029/2005GL022469, 2005.

Fahey, D. W., Eubank, C. S., Hübler, G., and Fehsenfeld, F. C.: A calibrated source of N_2O_5, Atmos. Environ., 19, 1883–1890, 1985.

Fried, A., Henry, B. E., Calvert, J. G., and Mozurkewich, M.: The Reaction Probability of N2O5 With Sulfuric-Acid Aerosols At Stratospheric Temperatures and Compositions, J. Geophys. Res., 99, 3517–3532, 1994.

Fuchs, N. A. and Sutugin, A. G.: Higly dispersed aerosols, Ann Arbor Sci., Ann Arbor, 1970.

Gobbi, G. P., Barnaba, F., Giorgi, R., and Santacasa, A.: Altitude-resolved properties of Saharan dust event over the mediterranean, Atmos. Environ., 34, 5119–5127, 2000.

Gomes, L. and Gillette, D. A.: A comparison of characteristics of aerosol from dust storms in central Asia with soil-derived dust from other regions, Atmos. Environ., 27A, 2539–2544, 1993.

Grim, R. E.: Clay Mineralogy, McGraw-Hill, New York, 1953.

Gustafsson, R. J., Orlov, A., Badger, C. L., Griffiths, P. T., Cox, R. A., and Lambert, R. M.: A comprehensive evaluation of water uptake on atmospherically relevant mineral surfaces: DRIFT spectroscopy, thermogravimetric analysis and aerosol growth measurements, Atmos. Chem. Phys., 5, 3415–3421, 2005, http://www.atmos-chem-phys.net/5/3415/2005/.

Hanisch, F. and Crowley, J. N.: Heterogeneous reactivity of gaseous nitric acid on Al_2O_3, $CaCO_3$, and atmospheric dust samples: A Knudsen cell study, J. Phys. Chem., 105, 3096–3106, 2001a.

Hanisch, F. and Crowley, J. N.: The heterogeneous reactivity of gaseous nitric acid on authentic mineral dust samples, and on individual mineral and clay mineral components, Phys. Chem. Chem. Phys., 3, 2474–2482, 2001b.

Hanisch, F. and Crowley, J. N.: heterogeneous reactivity of NO and HNO_3 on mineral dust in the presence of ozone, Phys. Chem. Chem. Phys., 5, 883–887, 2003a.

Hanisch, F. and Crowley, J. N.: Ozone destruction on Saharan dust: An experimental investigation, Atmos. Chem. Phys., 3, 119–130, 2003b.

Heintz, F., Platt, U., Flentje, H., and Dubois, R.: Long-term observation of nitrate radicals at the Tor station, Kap Arkona (Ruegen), J. Geophys. Res., 101, 22 891–22 910, 1996.

Hendricks, J., Lippert, E., Petry, H., and Ebel, A.: Heterogeneous reactions on and in sulfate aerosols: Implications for the chemistry of the midlatitude tropopause region, J. Geophys. Res., 104, 5531–5550, 1999.

Hinds, W. C.: Aerosol Technology, John Wiley & Sons, New York, 1999.

Hu, J. H. and Abbatt, J. P. D.: Reaction probabilities for N_2O_5 hydrolysis on sulfuric acid and ammonium sulfate aerosols at room temperature, J. Phys. Chem. A, 101, 871–878, 1997.

Hwang, H. J. and Ro, C. U.: Single-particle characterization of four aerosol samples collected in ChunCheon, Korea, during Asian dust storm events in 2002, J. Geophys. Res., 110, D23201, doi:10.1029/2005JD006050, 2005.

Immler, F. and Schrems, O.: Vertical profiles, optical and microphysical properties of Saharan dust layers determined by a shipborne lidar, Atmos. Chem. Phys., 3, 1353–1364, 2003, http://www.atmos-chem-phys.net/3/1353/2003/.

Karagulian, F. and Rossi, M.J.: The heterogeneous chemical kinetics of NO_3 on atmospheric mineral dust surrogates, Phys. Chem. Chem. Phys., 7, 3150–3162, 2005.

Karagulian, F., Santschi, C., and Rossi, M. J.: The heterogeneous chemical kinetics of N_2O_5 on $CaCO_3$ and other atmospheric mineral dust surrogates, Atmos. Chem. Phys., 6, 1373–1388, 2006, http://www.atmos-chem-phys.net/6/1373/2006/.

Keyser, L. F., Moore, S. B., and Leu, M.-T.: Surface-Reaction and Pore Diffusion in Flow-Tube Reactors, J. Phys. Chem., 95, 5496–5502, 1991.

Levin, Z., Price, C., and Ganor, E.: The contribution of sulfate and desert aerosols to the acidification of clouds and rain in Israel, Atmos. Environ., 24A, 1143–1151, 1990.

Lovejoy, E. R. and Hanson, D. R.: Measurement of the kinetics of reactive uptake by submicron sulfuric-acid particles, J. Phys. Chem., 99, 2080–2087, 1995.

Loyë-Pilot, M. D., Martin, J. M., and Morelli, J.: Influence of Saharan dust on the rain acidity and atmospheric input to the Mediterranean, Nature, 321, 427–428, 1986.

Lunt, D. J. and Valdes, P. J.: The modern dust cycle: Comparison of model results with observations and study of sensitivities, J. Geophys. Res., 107, 4669, doi:10.1029/2002JD002316, 2002.

Luo, C., Mahowald, N. M., and del Corral, J.: Sensitivity study of meteorological parameters on mineral aerosol mobilization, transport, and distribution, J. Geophys. Res., 108, 4447, doi:10.1029/2003JD003483, 2003.

Martinez, M., Perner, D., Hackenthal, E. M., Kulzer, S., and Schutz, L.: NO_3 at Helgoland during the NORDEX campaign in October 1996, J. Geophys. Res., 105, 22 685–22 695, 2000.

Matsuki, A., Iwasaka, Y., Shi, G. Y., Zhang, D.Z., Trochkine, D., Yamada, M., Kim, Y.S., Chen, B., Nagatani, T., Miyazawa, T., Nagatani, M., and Nakata, H.: Morphological and chemical modification of mineral dust: Observational insight into the heterogeneous uptake of acidic gases, Geophys. Res. Lett., 32, L22806, doi:10.1029/2005GL0244176, 2005.

Meskhidze, N., Chameides, W. L., and Nenes, A.: Dust and pollution: A recipe for enhanced ocean fertilization?, J. Geophys. Res., 110, D03301, doi:10.1029/JD005082, 2005.

Monchick, L. and Mason, E. A.: Transport properties of polar gases, J. Chem. Phys., 35, 1676–1697, 1961.

Mori, I., Nishikawa, M., Tanimura, T., and Quan, H.: Change in size distribution and chemical composition of kosa (Asian dust) aerosol during long-range transport, Atmos. Environ., 37, 4253–4263, 2003.

Nishikawa, M. and Kanamori, S.: Chemical composition of kosa

aerosol (yellow sand dust) collected in Japan, Anal. Sci., 7, 1127–1130, 1991.

Okada, K., Kobayashi, A., Iwasaka, Y., Naruse, H., Tanaka, T., and Nemoto, O.: Features of individual Asian dust storm particles collected at Nagoya, Japan, J. Met. Soc. Japan, 65, 515–521, 1987.

Phadnis, M. J. and Carmichael, G. R.: Numerical investigation of the influence of mineral dust on the tropospheric chemistry of East Asia, J. Atmos. Chem., 36, 285–323, 2000.

Prospero, J. M.: Mineral and sea-salt concentrations in various ocean regions, J. Geophys. Res., 84, 725–731, 1979.

Prospero, J. M. and Nees, R. T.: Impact of the North African drought and El Niño on mineral dust in the Barbados trade winds, Nature, 320, 735–738, 1986.

Reus, D. M., Dentener, F., Thomas, A., Borrmann, S., Strom, J., and Lelieveld, J.: Airborne observations of dust aerosol over the North Atlantic Ocean during ACE 2: Indications for heterogeneous ozone destruction, J. Geophys. Res., 105, 15 263–15 275, 2000.

Sander, S. P., Friedl, R. R., Golden, D. M., Kurylo, M. J., Huie, R. E., Orkin, V. L., Moortgat, G. K., Ravishankara, A. R., Kolb, C. E., Molina, M. J., and Finlayson-Pitts, B. J., Chemical kinetics and photochemical data for use in atmospheric studies: Evaluation Number 15, Jet Propulsion Laboratory, National Aeronautics and Space Administration/Jet Propulsion Laboratory/California Institute of Technology, Pasadena, CA, 2006.

Sassen, K., DeMott, P. J., Prospero, J. M., and Poellot, M. R.: Saharan dust storms and indirect aerosol effects on clouds: CRYSTAL-FACE results, Geophys. Res. Lett., 30, 1633, doi:10.1029/2003GL017371, 2003.

Seisel, S., Borensen, C., Vogt, R., and Zellner, R.: Kinetics and mechanism of the uptake of N_2O_5 on mineral dust at 298 K, Atmos. Chem. Phys., 5, 3423–3432, 2005, http://www.atmos-chem-phys.net/5/3423/2005/.

Shon, Z. H., Kim, K. H., Bower, K. N., Lee, G., and Kim, J.: Assessment of the photochemistry of OH and NO_3 on Jeju Island during the Asian-dust-storm period in the spring of 2001, Chemosphere, 55, 1127–1142, 2004.

Silva, P. J., Carlin, R. A., and Prather, K. A.: Single particle analysis of suspended soil dust from Southern California, Atmos. Environ., 34, 1811–1820, 2000.

Song, C. H. and Carmichael, G. R.: Gas-particle partitioning of nitric acid modulated by alkaline aerosol, J. Atmos. Chem., 40, 1–22, 2001.

Tegen, I., Harrison, S. P., Kohfeld, K., Prentice, I. C., Coe, M., and Heimann, M.: Impact of vegetation and preferential source areas on global dust aerosol: Results from a model study, J. Geophys. Res., 107, 4567, doi:10.1026/2001JD000963, 2002.

Twomey, S. A., Piepgrass, M., and Wolfe, T.: An assessment of the impact of pollution on global cloud albedo, Tellus, 36B, 243–249, 1984.

Wayne, R. P., Barnes, I., Biggs, P., Burrows, J. P., Canosa-Mas, C. E., Hjorth, J., Le Bras, G., Moortgat, G. K., Perner, D., Poulet, G., Restelli, G., and Sidebottom, H.: The nitrate radical: Physics, chemistry, and the atmosphere, Atmos. Environ., 25A, 1–206, 1991.

Wood, E. C., Bertram, T. H., Wooldridge, P. J., and Cohen, R. C.: Measurements of N_2O_5, NO_2 and O_3 east of the San Francisco Bay, Atmos. Chem. Phys., 5, 483–491, 2005, http://www.atmos-chem-phys.net/5/483/2005/.

Zasypkin, A. Y., Grigoreva, V. M., Korchak, V. N., and Gershenson, Y. M.: A formula for summing of kinetic resistances for mobile and stationary media: 1. Cylindrical reactor, Kinet. Catal., 38, 772–781, 1997.

Zhang, Y., Sunwoo, Y., Kotamarthi, V., and Carmichael, G. R.: Photochemical oxidant processes in the presence of dust: An evaluation of the impact of dust on particulate nitrate and ozone formation, J. Appl. Met., 33, 813–824, 1994.